Applied Catalysis B: Environmental 220 (2018) 429–445

Contents lists available at ScienceDirect

Applied Catalysis B: Environmental

journal homepage: www.elsevier.com/locate/apcatb

Review

Oxidative dehydrogenation of propane to propylene with carbon dioxide

Marktus A. Atanga[a], Fateme Rezaei[a], Abbas Jawad[a], Mark Fitch[b], Ali A. Rownaghi[a,*]

[a] Department of Chemical and Biochemical Engineering, Missouri University of Science and Technology, Rolla, MO 65409-1230, USA
[b] Department of Civil, Architectural and Environmental Engineering, Missouri University of Science and Technology, Rolla, MO 65409, USA

ARTICLE INFO

Keywords:
Carbon dioxide
Oxidative dehydrogenation
ODP reaction
Propane
Propylene

ABSTRACT

Oxidative dehydrogenation of propane in the presence of carbon dioxide (ODPC) is a sustainable approach and an attractive catalytic route for propylene production with less environmental footprint than the conventional oxidative dehydrogenation path with oxygen. Researchers have considered CO_2 as a mild oxidant that can overcome the problems of over-oxidation and low propylene selectivity, that are typically associated with the current synthesis routes. This article provides a critical review on the current mechanistic understanding of three different catalyst types used in the ODPC reaction based on experimental studies; (i) zeolites with different frameworks, (ii) porous materials-supported metal oxides, and (iii) transition metal oxides and other metal catalysts. A detailed review of the literature compares the framework, pore structure, nature of active sites, reducibility, and the role of promoters and supports for each type of catalytic materials in the absence and presence of CO_2, and is followed by a thorough discussion on the promotional effects of CO_2 as a soft oxidant on C—H bond scission. Future directions with respect to materials design, synthesis and reaction conditions are also discussed.

1. Introduction and motivation

Selective dehydrogenation of propane to propylene is one of the major challenges for production of valuable and versatile chemical feedstocks. The current industrial on-purpose propylene production through dehydrogenation of ethane and propane is non-oxidative in nature and is contributing to quick catalyst deactivation, low conversion and selectivity, and high reaction temperatures [1]. The current state-of-the-art research has primary focused on investigating the synergistic effects between gas phase oxidants and alkanes in order to overcome the hindrances in current industrial dehydrogenation reactions [2–5]. It is established that catalytic oxidative dehydrogenation (ODH) reactions are sensitive to specific oxidants [6,7]. A number of oxidants such as oxygen [6,8], nitrous oxide [6,9] and carbon dioxide [10,11] have been considered as co-feed in propane dehydrogenation reactions. Although, oxidative dehydrogenation of propane (ODP) in the presence of molecular O_2, as an oxidizing agent, favors low temperature reactions and is exothermic with no thermodynamic limitations [12,13], deep oxidation of propane and propylene to CO_x is a major drawback, which often results in loss of propylene selectivity and yield [13–15]. To address these issues, an alternative approach has been proposed by which O_2 is replaced with a milder oxidant such as CO_2 to convert propane to propylene over various heterogeneous catalysts.

Most experts studying the global ecosystem and climate suggest that rising anthropogenic CO_2 emissions have contributed to significant global climate change in the last half-century [16–21]. The development of effective strategies that convert such CO_2 emissions into energy, fuels, and chemicals are greatly preferable to oceanic or geologic sequestration options because they offer the potential to create new commercially-viable products from renewable carbon feedstock in a sustainable manner [2,22–24]. However, CO_2 is a thermodynamically stable molecule ($\Delta G_f = -394\ kJ\ mol^{-1}$) with a high oxidation state, hence, reactions of CO_2 must be combined with a high-energy reactant, effective catalysts and reaction conditions to gain a thermodynamic driving force [24,25].

The objective of this paper is to provide a critical review of the state-of-the-art materials that have been investigated for catalyzing the ODP reaction with CO_2 (ODPC) in order to establish a useful guideline for extrapolating and normalizing the reported ODPC reaction data to identify correlations between catalyst properties and performance. Among heterogeneous catalysts studied for the ODPC reaction so far, zeolites with the MFI and CHA frameworks, chromium- [26,27], platinum- [28,29], vanadium- [6,30] and gallium-based catalysts [31,32] are found to be the most efficient materials mainly due to their high activity and easy regeneration [33,34]. Literature shows that the catalytic activity of these materials depends upon various factors including the nature of support [10], promoters [35], and the synthesis

* Corresponding author.
E-mail addresses: ali.rownaghi@gmail.com, rownaghia@mst.edu (A.A. Rownaghi).

http://dx.doi.org/10.1016/j.apcatb.2017.08.052
Received 14 May 2017; Received in revised form 6 August 2017; Accepted 15 August 2017
Available online 19 August 2017

procedures [36,37]. Therefore, in this review, we will focus on reviewing the effects of CO_2 partial pressure, acid-based properties and porosity of different zeolites, metal oxides reducibility and bifunctional catalysts (*i.e.*, metal-supported zeolites) on the conversion of propane, selectivity of propylene, and the kinetics of the ODPC reaction. In addition, the effect of process conditions on the ODPC reaction is discussed and future research directions are provided.

2. Oxidative dehydrogenation of propane with O_2 and CO_2

Despite the extra ordinary effect of molecular O_2 (exothermicity and equilibrium support effect), deep oxidation of products has been confirmed even at small doses of O_2, resulting in reduced selectivity to propylene. Aside from this deep oxidation, the high exothermicity of O_2 generates great amount of energy that must be removed [1,13,31]. In general, the major drawback of ODP with O_2 is that the propylene yield is typically low on a laboratory scale, as stated above, and that the role of catalysts and their fast deactivation in the presence of O_2 are not well-understood [12,13,38]. For instance, by reviewing the literature in the period of 1995–2017, the best propylene yield of 40% has been reported for ODP with O_2 which is still far from industrial implementation and the information concerning the catalyst lifetime appeares quite limited [1,13,27,39–42]. The scale-up of catalytic materials and/or reactor configurations capable of maintaining high selectivity to propylene under conditions leading to high propane conversion is another aspect that has been often overlooked.

A comprehensive review of the literature on the dehydrogenation of light alkanes that covers exclusively metal and metal-oxide catalysts has been undertaken by Sattler et al. [1]. Their review provided a summary of parameters including nature of active sites, type of supports and promoters, and feed composition, affecting the catalytic properties and lifetime of systems based on GaO_x, VO_x, MoO_x, Pt and Pt-Sn, and CrO_x supported catalysts [1]. In other reviews, Pt-based catalysts have been discussed from the perspective of catalyst design [43], mass transfer limitations, and the influence of hydrogen combustion on olefin yield [44]. Albonetti et al. [45] discussed the chemistry of vanadium in ODP reaction in their review. Cavani et al. [38] compiled a review on over 100 catalysts with different active phases for the ODP reaction with O_2 as a co-feed. In that review, features of catalysts with remarkable performance, reaction network of partial and total oxidation, and the influence of homogenous gas phase reactions on the formation of olefins in ODH of alkanes were covered [38]. Recently, Carrero et al. [13] reviewed the kinetics of ODP over VO_x catalysts with the focus on the effects of catalyst synthesis method, molecular structure of supported vanadium oxide species, reaction mechanism, and structure-activity relationship of the vanadium-based catalysts.

Several other reviews exist on the ODH of alkanes with CO_2. For instance, Krylov et al. [46] reviewed the oxidation of hydrocarbons and alcohols with CO_2 over manganese oxide catalysts in 1995. The authors concluded that manganese oxide-based catalysts are active, selective, and do not form a carbon layer during the reaction in dry reforming of methane and oxidative dehydrogenation of C_2–C_7 hydrocarbons and the lower alcohols. Another mini-review by Wang et al. [40] discussed dry reforming of methane and dehydrogenation of light alkanes in the presence of CO_2, more than a decade and half ago. The information in that review was limited to CH_4, with no in-depth discussion on C_2H_6 and C_3H_8 conversion and no consideration of microporous materials such as zeolites [40]. Other notable reviews on the use of CO_2 as a mild oxidant for the dehydrogenation of alkanes, especially ethylbenzene and methane in the presence of CO_2 have been provided by Ansari and Park [2] and Kawi et al. [24].

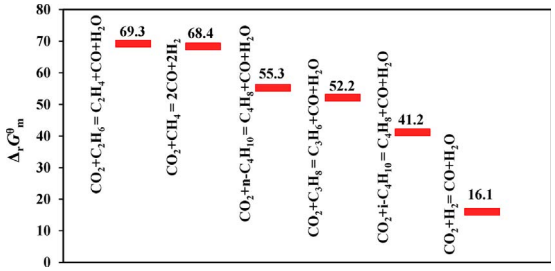

Fig. 1. $\Delta_r G^\theta_m$ of the reactions between CO_2 and light alkanes at 400 °C and normal pressure [5,25].

3. Thermodynamic analysis of dehydrogenation of light alkanes with CO_2

Recently, the use of CO_2 in oxidative dehydrognation of light alkanes has received significant attention as it has been shown to shift the ODH reaction toward more olefin production compared to molecular O_2 by preventing deep oxidation of the reaction products and as a coke removal agent from the catalyst [47,48]. As shown in Fig. 1, the Gibbs free energy changes of CO_2 ($\Delta_r G^\theta_m$) reaction becomes increasingly favorable by moving towards higher alkanes.

Recently, Edwards et al. [25] investigated the effect of temperature and CO_2 on the Gibbs free energy for dehydrogenation of light alkanes from 300 to 500 °C and reported that although all ODH reactions of light alkanes with CO_2 show a similar trend, ethane dehydrogenation displays the highest $\Delta_r G^\theta_m$ (Fig. 1), indicating that it is much harder to operate this reaction as compared to propane and butane dehydrogenation reactions at 300–500 °C. Furthermore, the dehydrogenation of propane with CO_2 was more favorable than *n*-butane but less feasible than *i*-butane, as shown in Fig. 2. The butane has multiple curves because of its constituent isomers. Therefore, $\Delta_r G^\theta_m$ does not keep falling as the carbon number of alkane increases and lower value of $\Delta_r G^\theta_m$ indicates a higher possibility of cracking. The authors also studied the $\Delta_r G^\theta_m$ of light alkanes and olefins cracking to generate carbon and H_2 and found that (i) olefins show a much higher cracking possibility than alkanes, (ii) propylene has a much higher resistance to cracking than any isomers of butane, (ii) the selectivity of the target products is significantly affected by further cracking of the olefin. As can be seen from Fig. 3a, although ethylene has higher resistance to subsequent cracking compared to propylene, it is more difficult for ethane to be activated with CO_2 when the temperature is kept below 500 °C (Fig. 3a). Therefore, from thermodynamics perspective, the ODPC is the best dehydrogenation pathway below 500 °C in comparison to other alkanes.

In general, alkanes dehydrogenation reactions with CO_2 are very complicated because they are thermodynamically limited at low

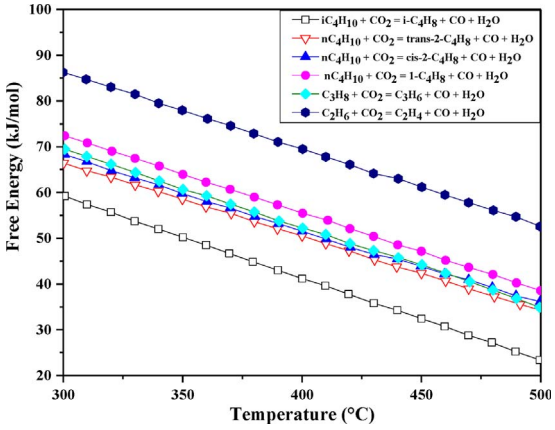

Fig. 2. $\Delta_r G^\theta_m$ of the ODH of light alkanes in the presence of CO_2 at 300–500 °C [25].

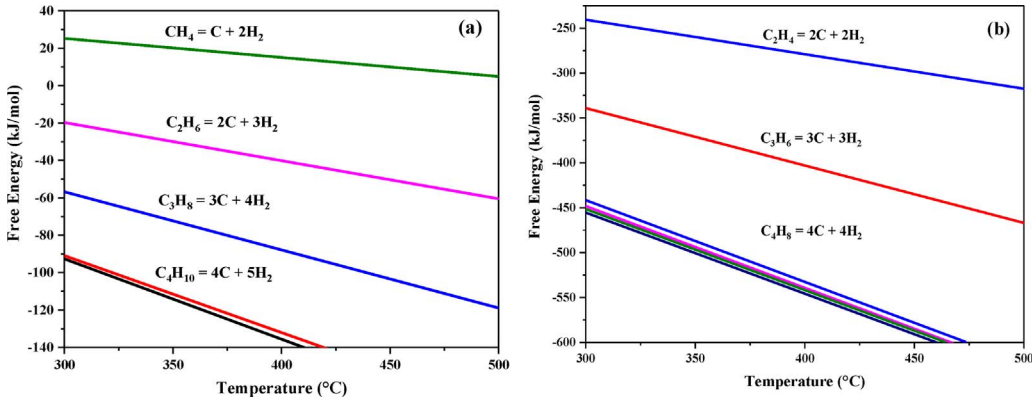

Fig. 3. $\Delta_r G_m^\theta$ of (a) light alkanes and (b) olefins cracking in temperature range of 300–500 °C [25].

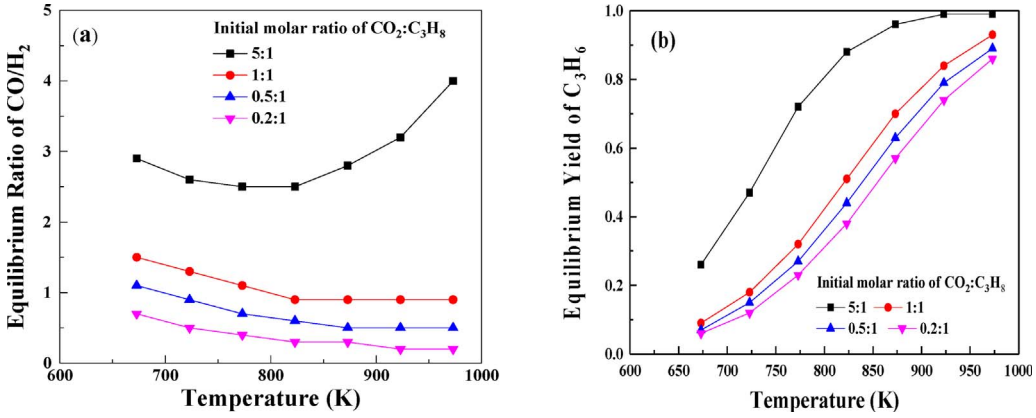

Fig. 4. Effect of temperature and CO_2/C_3H_8 molar ratio on (a) equilibrium molar ratio of CO/H_2 and (b) yield of propylene [37].

temperatures and high pressures. Much of the discussion is presented in terms of ODPC since the dehydrogenation mechanisms and kinetics of other alkanes such as ethane, butanes and ethylbenzene are not quite different [2,4,5,24,37,46]. Propane interaction with CO_2 can proceed on different catalysts by various reaction pathways and associated side reactions, as presented in Eqs. (1)–(9). The production of hydrogen in the non-oxidative dehydrogenation of propane (Eq. (1)) limits the conversion of the propane by shifting the thermodynamic equilibrium to the reactant side [49,50]. However, by coupling this reaction with CO_2 through the reverse water-gas shift (RWGS) reaction (Eq. (2)) [36,51,52] the imposed limitation is removed by shifting the equilibrium position to the product side, thereby increasing the yield of propylene [10,27,36]. Moreover, the RWGS reaction accelerates the formation of the dehydrogenation products by transforming H_2 with CO_2 into CO and H_2O, while promoting desorption of ethylene from the catalyst surface [53,54]. It has also been accepted that CO_2 directly participates in the ODP reaction (Eq. (3)) which further enhances the propylene formation (ODPC). In addition, CO_2 can stabilize the catalyst by eliminating coke through the reverse Boudouard reaction (Eq. (4)) [54,55]. Nonetheless, dry reforming of propane (Eq. (5)) which produces syngas (CO/H_2) may take place as a competing side reaction, although such a reaction is highly endothermic (ΔH_{298K} = + 620 kJ mol^{-1}) and preferentially takes place at high temperatures [56–58]. In addition, depending on the type of catalyst used, other side reactions such as propane cracking and hydrogenolysis reactions (Eqs. (6)–(9)) become dominant at high temperatures where thermodynamics favor conversions, and thus selectivity toward the desired product (*i.e.* propylene) decreases [54,59–61].

$$C_3H_8 \leftrightarrow C_3H_6 + H_2 \qquad \Delta H_{298\ K} = +124\ kJ\ mol^{-1} \quad (1)$$

$$CO_2 + H_2 \leftrightarrow CO + H_2O \qquad \Delta H_{298\ K} = +41\ kJ\ mol^{-1} \quad (2)$$

$$C_3H_8 + CO_2 \leftrightarrow C_3H_6 + CO + H_2O \qquad \Delta H_{298\ K} = +164\ kJ\ mol^{-1} \quad (3)$$

$$CO_2 + C \leftrightarrow 2CO \qquad \Delta H_{298\ K} = +172\ kJ\ mol^{-1} \quad (4)$$

$$C_3H_8 + 3CO_2 \leftrightarrow 6CO + 4H_2 \qquad \Delta H_{298\ K} = +620\ kJ\ mol^{-1} \quad (5)$$

$$2C_3H_8 + 2CO_2 \rightarrow 3C_2H_4 + 2CO + 2H_2O \quad (6)$$

$$C_3H_8 \rightarrow C_2H_4 + CH_4 \quad (7)$$

$$C_3H_8 + H_2 \rightarrow C_2H_6 + CH_4 \quad (8)$$

$$C_3H_8 + 2H_2 \rightarrow 4CH_4 \quad (9)$$

Although ODPC reaction is endothermic in nature ($\Delta H_{298\ K}$ = + 164 kJ mol^{-1}) as opposed to ODP with O_2 ($\Delta H_{298\ K}$ = −120 kJ mol^{-1}), in this reaction CO_2 will be a great co-feed from both an economic and ecological point of view. This is mainly because CO_2 can serve myriad purposes by enhancing equilibrium conversion of light alkanes by removing hydrogen through the RWGS reaction (Eq. (2)) [62], acting as an agent for coke removal through the reverse Boudouard reaction (Eq. (4)) [31,62], and ensuring recycling of greenhouse gas, and eliminating deep oxidation [14,27,34,36,63].

Through thermodynamic calculations, Michorczyk et al. [37] noted that the syngas composition (CO/H_2 molar ratio) and the yield of C_3H_6 can be manipulated by changing the molar ratio of CO_2 to C_3H_8 in the feed and reaction temperature, as shown in Fig. 4a and b. It is apparent from Fig. 4a that the equilibrium CO/H_2 ratio increases significantly with the amount of CO_2 in the feed, but decreases approximately linearly with temperature, except for the CO_2/C_3H_8 ratio of 5 where the equilibrium syngas ratio demonstrates a nearly quadratic relationship with temperature. However, as shown in Fig. 4b, the yield of C_3H_6 increases drastically with both temperature and CO_2/C_3H_8 molar ratio, with significantly higher yields at a feed ratio of 5. One can therefore expect to achieve higher C_3H_6 yield in the ODPC reaction at low temperatures by simply varying the CO_2/C_3H_8 feed molar ratio. Nonetheless, the negative effect of CO_2 displacing ethane adsorbed on the

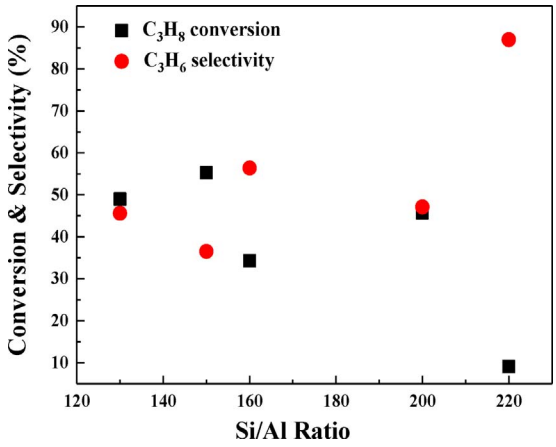

Fig. 5. Effect of Si/Al ratio on the performance of Ga_2O_3/ZSM-48 catalysts for ODPC reaction [84].

catalyst surface has also been reported [53].

4. Oxidative dehydrogenation of propane with CO_2 (ODPC)

With the expected high future demand for propylene, commercialization of oxidative dehydrogenation reactions that uses CO_2 will not only meet the demand for propylene, it will also go a long way to support combatting climate change. As pointed out earlier, the nature of CO_2 interaction differs from catalyst to catalyst. The RWGS reaction can proceed only when both H_2 and CO_2 are adsorbed on the catalyst surface. Therefore, an effective catalyst for ODPC should have affinity for both CO_2 and C—H over C—C bond cleavage to avoid side reactions. Moreover, as CO_2 is slightly acidic, it would preferentially adsorb onto the basic sites of catalyst while propane and H_2 adsorb on the acidic sites, thus a balance of acidity and basicity is required to avoid unwanted side and secondary reactions including propane hydrogenolysis, thermos and catalytic cracking, and isomerization reaction.

To date, unusual contrasting effects of CO_2 on the performance of catalyst supports used in ODP have been reported. These contrasting effects are not clarified and researchers have not yet reached a conclusion on the exact role of CO_2 in the propane dehydrogenation reaction. For instance, Nakagawa et al. [31] proposed that CO_2 promotes desorption of propylene product from the catalyst surface while Michorczyk et al. [64] found that CO_2 consumes H_2 *via* the RWGS reaction. For Ga_2O_3/TiO_2, CO_2 is consumed mainly through the RWGS reaction, which may account for the enhancement of the dehydrogenation activity, whereas for Ga_2O_3/ZrO_2, the main role of CO_2 is the elimination of coke, which may account for the enhancement of stability of the catalyst after the addition of CO_2 [56,65]. This can be attributed to the higher density of surface basicity due to terminal hydroxyl groups (strong Lewis acidity of Zr^{4+} and the Lewis basicity of O^{2-} pairs) on ZrO_2 structure that results in higher CO_2 adsorption and consequently coke elimination through reverse Boudourd reaction [66,67]. Contrary observations were made in the case of Al_2O_3 [66,67]. Therefore, in the design and development of new materials for the ODPC reaction, the interaction of CO_2 with catalyst active sites should be thoroughly investigated through *in-situ* or *ex-situ* experimental measurements and/or theoretical studies. In this section, we will review the ODPC reaction over various heterogeneous catalysts.

4.1. Oxidative dehydrogenation of propane with CO_2 over zeolites

The catalytic performance of a zeolite is largely dictated by its framework topology, particle size, and acidity [68–73]. Mass transport to and from the active sites located within the micropores of the zeolite is usually slow, which results in longer residence time that could increase propylene oligomerization and coke formation [74,75]. It is a wide consensus that propane dehydrogenation activities occur on acid sites of zeolite. Also, the SiO_2/Al_2O_3 ratio plays a major role in both the zeolite physicochemical and reactivity properties [76–80]. The inverted mordenite framework (MFI) zeolites such as HZSM-5 and mesoporous silica materials (*e.g.* MCM-41 [81], SBA-1 [26], SBA-15 [73] and MSU-x [82]) provide a two-dimensional channel network intersecting microchannels with a 5–6 Å size. These materials have been widely evaluated in ODH of light alkanes with CO_2. Zhang et al. [83] prepared Na-HZSM-5 with 400 nm (HZSM-5-S) and 2 μm (HZSM-5-L) crystal sizes impregnated with chromium oxide and utilized for ODPC reaction at 550 °C. The sub-microsize catalyst (ca. 400 nm) exhibited substantially higher activity than HZSM-5 with larger crystal size (ca. 2 μm). In addition, the authors studied the promotional effect of promoters such as Cr^{+6} in the presence and absence of CO_2 over HZSM-5 catalysts for the ODP reaction. The initial propane conversion and propylene selectivity were 48.3% and 86.0% over Cr/HZSM-5-S and 11.3% and 92.8% over and Cr/HZSM-5-L, respectively. After 8 h on stream, these values decreased to 30.1% and 91.8% for the former catalyst and 8.4% and 94.1% for the later catalyst, respectively. Combined Raman, diffuse reflectance UV–vis, XPS, and H_2-TPR results demonstrated that the submicrosize catalyst has much higher concentration of surface Cr^{6+} species than the microsize catalyst, which accounts for its superior catalytic performance. In addition to the coke formation, the reduction of monochromate Cr^{6+} to polychromates Cr^{3+} affected the catalyst deactivation and that the catalyst can be regenerated by re-oxidizing Cr^{3+} and burning carbon deposits.

The effect of surface acidity on the performance of zeolites in the ODPC reaction has been investigated by several research groups. As shown in Fig. 5, with increasing Si/Al ratio of HZSM-5 supported Ga_2O_3, the activity of the catalyst decreased but the selectivity increased comparably [84]. The decrease in BrØnsted acidity was much higher than that of Lewis acidity due to the fact that Lewis acidity is associated with Ga_2O_3 while BrØnsted acidity is associated with HZSM-5, thus removing the aluminum from HZSM-5 consequently decreases the BrØnsted acidity. In the same study, Ren et al. [84] reported the catalytic performance of Ga_2O_3 supported HZSM-48 catalysts for ODPC reaction. The performance with changing Si/Al ratio was similar to the above observations, however, Ga_2O_3/HZSM-48 with Si/Al ratio of 130 showed the best propylene yield of 22.2%. The selectivity of propylene on Ga_2O_3/HZSM-48 was higher than that over Ga_2O_3/HZSM-5, especially at low propane conversion, due to its weaker acidity. However, the stability on Ga_2O_3/HZSM-48 was lower compared to Ga_2O_3/HZSM-5, which may be caused by its abundant weak acid sites and unidimensional pore structure.

In another investigation, Ren et al. [86] reported similar observations for the effect of Si/Al ratio on the behavior of HZSM-5 supported ZnO catalysts in ODPC reaction. The initial activity of ZnO/HZSM-5 catalysts decreased with increasing the Si/Al ratio, while stability and propylene selectivity were both enhanced during ODPC reaction (Fig. 6). The ZnO/HZSM-5 with Si/Al = 160 displayed the best performance with a propane conversion of 41.5% and propylene yield of 25.8% at steady state reaction. The enhancement of the catalyst stability with increasing the Si/Al ratio of the HZSM-5 support was ascribed to the decrease of the acidity of the catalysts, which led to the suppression of the side reactions such as cracking, oligomerization, and aromatization.

In another study, Zhu et al. [85] evaluated the ODPC reaction over a series of Cr-based catalysts supported on MFI zeolitic materials. The catalysts Cr/silicalite-1 and Cr/H[B]MFI were prepared by the impregnation method, while Cr/H[B]MFI was further treated by steaming. Significantly higher activity was obtained for Cr/H[B]MFI than Cr/silicalite-1, and steamed Cr/H[B]MFI was superior in the reaction stability to Cr/H[B]MFI. It was suggested that the boron present in the framework modified the nature of introduced Cr species and the steaming process resulted in auto-reduction of some Cr^{6+} to Cr^{3+} on

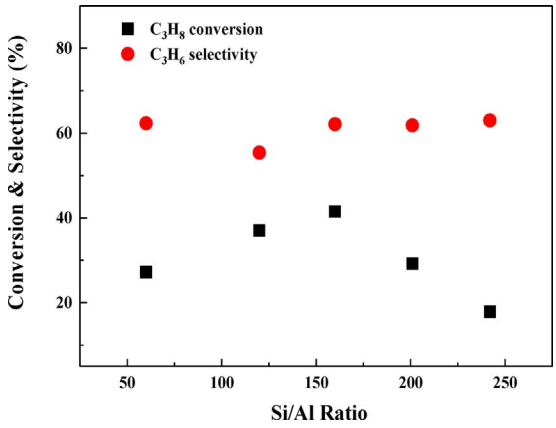

Fig. 6. Effect of Si/Al ratio on the performance of ZnO-HZSM-5 catalysts in ODPC reaction [86].

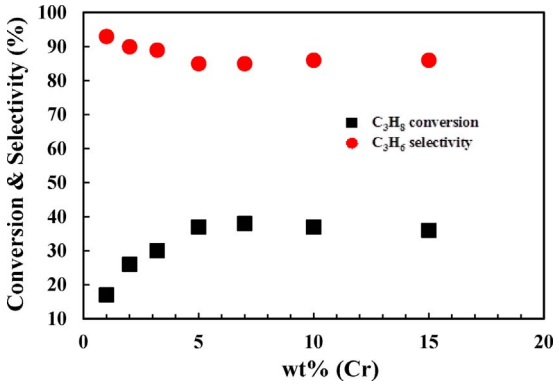

Fig. 7. Effect of Cr content on the performance of Cr/SBA-15 in the presence of CO_2 [26].

Cr/H[B]MFI. The enhanced stability of the steam-treated catalyst was associated to Cr^{3+} oxide species, which are perceived to be more reactive than Cr^{3+} from reduced Cr^{6+}. The list of metal supported MFI catalysts for ODPC reaction as well as the catalytic evaluation results and the corresponding reference papers are summarized in Table 1.

Several recent investigations have indicated that Cr-containing mesoporous sieves have excellent catalytic activity in ODPC reaction [26,88,89]. Michorczyk et al. [26,88] incorporated various amounts of chromium (1–15 wt%) into SBA-1 to make a series of Cr/SBA-1 catalysts with highly ordered cubic structure and high specific surface area (S_{BET} > 900 $m^2 g^{-1}$) up to Cr/Si = 0.06 atomic ratio. Their observations and that of Baek et al. [89] confirmed that activity of the catalysts increased with Cr content to an optimum loading of 4.3 wt%, as shown in Fig. 7. Unlike the regular wet impregnation process in which the Cr sits on the surface and pore mouths of the support, the incorporation method enhanced the distribution of the Cr species within the channels and framework of the catalyst, thereby increasing the BET surface area. The dehydrogenation activity was shown to be proportional to the number of redox chromium species. Michorczyk's group [26] further investigated the characteristics of Cr/SBA-1 using *in-situ* UV–vis DR analysis. Results obtained during ODPC reaction revealed that the Cr^{6+} species were already reduced rapidly at the beginning of the process. On the basis of their obtained results, the authors concluded that the resultant Cr^{2+} and Cr^{3+} species trigger redox cycles responsible for high catalytic activity of the Cr/SBA-1 materials.

Digging deeper into the effect of metal promoters on catalytic performance of zeolites, researchers have found that Sn added to Pt-HZSM-5 reduces coke formation by suppressing side reactions [90]. As a consequence, it increases catalyst stability, dispersion of Pt by its geometrical effect and the catalyst activity. As shown in Table 2, the addition of Na, La, and Mg can neutralize the strong acid sites on the surface of the catalysts and improve the synergy between the metals and the zeolite support [91]. Zhang et al. [60] confirmed these claims in their work where they co-impregnated Pt and Sn in HZSM-5 and further impregnated it with different amounts of K for propane dehydrogenation in the absence of CO_2. Characterization results confirmed that the addition of K improved the dispersion of Pt and the interaction between Pt and Sn, while decreased the amount of acid sites in the catalyst. This led to improved activity, selectivity, and stability of the catalysts, but the performance was deteriorated past an optimum

Table 1
Dehydrogenation of propane to propylene over metal supported MFI zeolites in the presence of CO_2.

Catalyst	Si/Al	S_{BET} m^2/g	Feed, vol% C_3H_8:CO_2:N_2	W/F g min mL^{-1}	TOS h	$X_{C_3H_8}$ %	X_{CO_2} %	$S_{C_3H_6}$ %	$Y_{C_3H_6}$ %	Refs.
Ga_2O_3/HZSM-48	130	252	2.5:5:92.5	0.01	10	49	–	46	22	[84]
Ga_2O_3/HZSM-48	160		2.5:5:92.5	0.01	10	34	–	56	19	[84]
Ga_2O_3/HZSM-48	220		2.5:5:92.5	0.01	10	9	–	87	7.9	[84]
Ga_2O_3/HZSM-5	150		2.5:5:92.5	0.01	10	55	–	37	20	[84]
Ga_2O_3/HZSM-5	200	394	2.5:5:92.5	0.01	10	45	–	47	22	[84]
ZnO/HZSM-5	60	337	2.5:5:92.5	0.01	30	27	–	62	17	[86]
ZnO/HZSM-5	120	341	2.5:5:92.5	0.01	30	37	–	55	20	[86]
ZnO/HZSM-5	160	312	2.5:5:92.5	0.01	30	41	–	62	26	[86]
ZnO/HZSM-5	201	344	2.5:5:92.5	0.01	30	29	–	62	18	[86]
ZnO/HZSM-5	242	300	2.5:5:92.5	0.01	30	18	–	63	11	[86]
Cr/HZSM-5	62	359	2.5:5:92.5	0.01	8	30	–	9.8	28	[86]
Cr/HZSM-5	63	356	2.5:5:92.5	0.01	8	84	–	94	79	[86]
Ga_2O_3/HZSM-5	240	385	2.5:5:92.5	0.01	50	48	–	45	22	[84]
Ga_2O_3/HZSM-5	173	344	2.5:5:92.5	0.01	30	53	–	41	22	[84]
Ga_2O_3/HZSM-5	180	–	2.5:5:92.5	0.01	30	37	–	54	20	[84]
1%Cr/SBA-1	–	1107	1:5:1:9	0.007	0.2	17	1.4	93	16	[26]
2%Cr/SBA-1	–	1084	1:5:1:9	0.007	0.2	26	2.8	90	23	[26]
3%Cr/SBA-1	–	1002	1:5:1:9	0.007	0.2	30	4	89	27	[26]
5%Cr/SBA-1	–	963	1:5:1:9	0.007	0.2	37	6.1	85	32	[26]
7%Cr/SBA-1	–	888	1:5:1:9	0.007	0.2	38	6.7	85	32	[26]
10%Cr/SBA-1	–	862	1:5:1:9	0.007	0.2	37	6.4	86	32	[26]
15%Cr/SBA-1	–	832	1:5:1:9	0.007	0.2	36	6.2	86	31	[26]
10 V/SBA-15/Al_2O_3/FeCrAl	–	–		0.01	12	40	7.8	83	34	[87]
10V-10Cr/SBA-15/Al_2O_3/FeCrAl	–	–	1:03:00	0.01	12	50	9.2	87	42	[87]

All reactions were carried out at 590–600 °C and 1 atm.
W/F = contact time; TOS = time on stream.
X = conversion; S = selectivity; Y = yield.

Table 2
Dehydrogenation of propane to propylene over metal supported MFI zeolites in the absence of CO_2.

Catalyst	Si/Al	S_{BET} m^2/g	Feed H_2/C_3H_8	WHSV h^{-1}	TOS h	$X_{C_3H_8}$ %	$S_{C_3H_6}$ %	$Y_{C_3H_6}$ %	Refs.
HZSM-5	140	–	0.25	5.6	1	29	21	6	[92]
Ga_2O_3/M-HZSM-5	240	385	0.025[a]	7	30	38	20	20	[84]
Ga_2O_3/M-HZSM-5	78	363	0.025[a]	7	10	58	36	21	[84]
Ga_2O_3/M-HZSM-5	144	336	0.025[a]	7	10	57	38	22	[84]
Ga_2O_3/M-HZSM-5	173	344	0.025[a]	7	10	56	39	22	[84]
Ga_2O_3/M-HZSM-5	240	385	0.025[a]	7	10	54	41	22	[84]
Ga_2O_3/M-HZSM-5	307	385	0.025[a]	7	10	49	43	21	[84]
Pt/HZSM-5	140	–	0.25	5.6	1	27	35	10	[92]
PtSn/HZSM-5	140	396	0.25	5.6	1	27	40	9	[92]
PtNa/HZSM-5	400	299	0.25	3	10	35	92	32	[93]
PtNaZn(0.5%)/HZSM-5	400	315	0.25	3	10	36	95	34	[93]
PtNaZn(1%)//HZSM-5	400	351	0.25	3	10	36	98	36	[93]
PtNaZn(1.5%)//HZSM-5	400	354	0.25	3	10	38	99	37	[93]
HZSM-5	20.2	275.7	0.8	4	5	28	70	20	[94]
PtSn/HZSM-5	0.24	298	0.25	3	8	27	34	11	[60]
PtSnK(0.2%)/HZSM-5	1.6	298	0.25	3	8	22	58	13	[60]
PtSnK(0.5%)/HZSM-5	5.5	296.7	0.25	3	8	25	89	23	[60]
PtSnK(0.8%)/HZSM-5	20.2	290.6	0.25	3	8	31	92	30	[60]
PtSnK(1%)/HZSM-5	–	289.5	0.25	3	8	21	94	21	[60]
PtSnK(1.2%)/HZSM-5	60	287.9	0.25	3	8	22	92	24	[60]
PtSnNa/HZSM-5 (400[c])	120	308	0.25	3	4	28	96	27	[95]
PtSnNa/HZSM-5 (500[c])	120	307.7	0.25	3	4	37	98	36	[95]
PtSnNa/HZSM-5 (600[c])	120	291.8	0.25	3	4	18	87	16	[95]
PtSnNa/HZSM-5 (700[c])	120	273.7	0.25	3	4	16	83	13	[95]
PtSnNa/HZSM-5 (800[c])	120	253	0.25	3	4	15	82	12	[95]
PtSnNa/HZSM-5 (0)[h]	120	335.4	0.25	3	6	34	98	33	[96]
PtSnNa/HZSM-5 (400[h])	120	326.1	0.25	3	6	32	99	32	[96]
PtSnNa/HZSM-5 (550[h])	120	301.6	0.25	3	6	22	96	21	[96]
PtSnNa/HZSM-5 (650[h])	120	278.7	0.25	3	6	12	90	11	[96]
PtSnNaLa/HZSM-5 (0[c])	400–333	–	0.25	3	8	31	98	30	[97]
PtSnNaLa/HZSM-5 (500[c])	400–333	–	0.25	3	8	31	98	31	[97]
PtSnNaLa/HZSM-5 (550[c])	400–333	–	0.25	3	8	32	98	31	[97]
PtSnNaLa/HZSM-5 (600[c])	400–333	–	0.25	3	8	33	97	33	[97]
PtSnNaLa/HZSM-5 (650[c])	400–333.	–	0.25	3	8	34	98	33	[97]
PtSnNaLa/HZSM-5 (700[c])	400–333	–	0.25	3	8	28	99	28	[97]
5 wt%Cr/SBA-1	–	963	5:1:9[d]	30	8	33	86	28	[26]

All reactions were carried at 590–600 °C, 1 atm.
DHS = Direct hydrothermal synthesis TOS = Time on stream; X = conversion; S = selectivity; Y = yield.
[a] = C_3H_8/N_2.
[h] = hydrothermal treatment temperature.
[c] = calcination temperature.
[d] = molar ratio of N_2:C_3H_8:He.

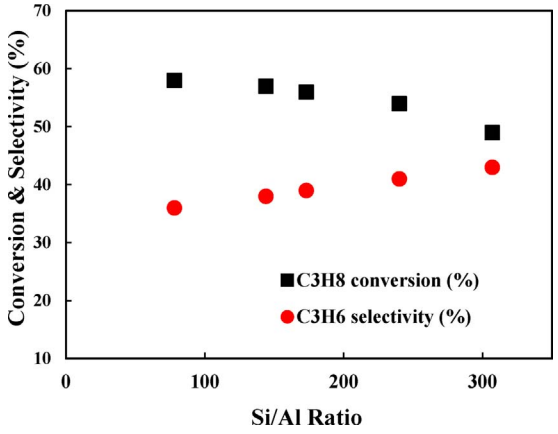

Fig. 8. Effect of Si/Al ratio on the performance of Ga_2O_3/M-HZSM-5 catalysts in the absence of CO_2 [84].

composition (ca. 0.8 wt% K), after which the activity and stability of the catalyst began to dwindle. At this composition of K, conversion as high as 33% with yield and selectivity of 30% and 91.43%, respectively, were obtained, which were higher than those over PtSn/HZSM-5 with 27.5% conversion, 12% yield and 37.3% selectivity after 8 h time on stream. Ren et al. [86] observed similar effects of Si/Al ratio in oxidative dehydrogenation of propane in the absence of CO_2 using Ga_2O_3 supported ZSM-5 catalysts. The initial activity of Ga_2O_3/M-HZSM-5 catalysts decreased with increasing the Si/Al ratio, while enhancing stability and propylene selectivity during ODP reaction (Fig. 8). The Ga_2O_3/M-HZSM-5 with Si/Al = 240 catalyst exhibited the best performance with a propane conversion of 54% and propylene selectivity of 41% at steady state reaction. The list of metal supported MFI materials for ODP reaction as well as the catalytic evaluation results and the corresponding reference papers are summarized in Table 2.

Zhang et al. [93] recently incorporated Zn into the framework of HZSM-5 by hydrothermal synthesis and used it as a support for Pt catalysts. Interestingly, the use of this Zn containing HZSM-5 resulted in the strong interactions between Pt and the support, thus leading to higher resistance towards reduction. PtNa/Zn (1.0%)-HZSM-5 exhibited the highest catalytic behavior with initial activity of 40.60% and the lowest deactivation parameter (7.3%) after reaction time of 10 h. However, with the increasing content of Zn. The formation of the PtZn alloy decreased the Pt dispersion and modified the metallic phase, which led to the decreased reaction activity and stability. Furthermore, the impregnation process decreased the surface area of zeolite catalysts due to pore blockages by the metal precursors [93]. Moreover, the introduction of metal into the framework of zeolites increased the surface area of zeolite support due to the formation of small crystal sizes. The same group

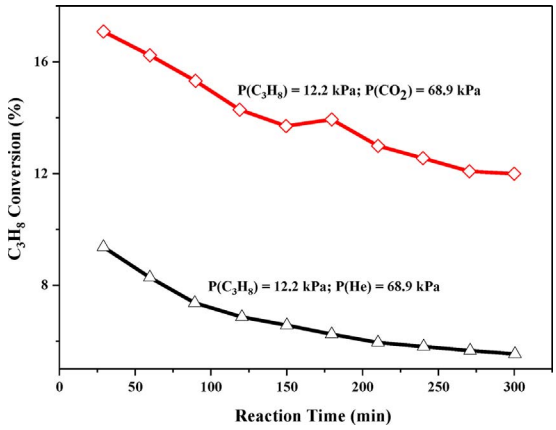

Fig. 9. Deactivation of Cr/MCM-41 (Si/Cr = 50) catalysts during the ODP reaction. Reaction conditions: catalyst weight, 400 mg; reaction temperature, 550 °C; $F = 0.134$ mol (STP) h^{-1} [36].

[98] had earlier reported similar behavior of isomorphous substitution of Sn in HZSM-5 and used it as a support for dispersing PtNa metals catalysts. In comparison with the conventional impregnated PtNa/HZSM-5 and PtSnNa/HZSM-5 catalysts, the Sn-modified HZSM-5-based Pt catalyst exhibited higher propane reaction activity and stability. Furthermore, it showed the lowest deactivation parameter (6.2%) and exhibited a selectivity to propylene higher than 98% with the corresponding propane conversion of about 39.0% after the reaction for 9 h [98]. At time on stream of l75 h, selectivity of 98.6% and yield of 30% were reported [98]. In a later investigation by the same group [97], it was demonstrated that calcining a La-doped PtSnNa/HZSM-5 can reduce dealumination of the HZSM-5 support and strengthen the interaction between Pt and Sn oxide, thereby resulting in improved performance of the catalyst in dehydrogenation of propane to propylene. In contrast to the catalyst without the calcination of La, the treatments in the range of 500–650 °C resulted in the strong interaction between La species and the support, thus suppressing the dealumination of the support and increasing interactions between Sn species and the support as well as Pt and Sn oxides. In the propane dehydrogenation test, the catalyst calcined at 650 °C of La showed the best reaction activity and stability. The average yield of propylene was about 34.3% over 82 h for the reaction of propane dehydrogenation at 590 °C. However, after the thermal treatment of La at 700 °C, a sharp decrease in catalyst acidity due to severe dealumination was observed. Meanwhile, sintering of Pt particles and the formation of Sn^0 species were found, which resulted in the deactivation of catalyst. In another investigation, the effect of CO_2 on the conversion of propane over Cr/MCM-41 catalysts was reported by Takehira et al. [36]. It was found that both C_3H_8 conversion and C_3H_6 yield increased two folds in presence of CO_2 (Fig. 9). The catalyst activity gradually decreased in presence and absence of CO_2 during the reaction over the Cr-MCM-41, indicating catalyst deactivation.

Nawaz and coworkers [92] compared the effect of Sn and Pt on the dehydrogenation properties of SAPO-34, a silicoaluminophosphate having chabazite (CHA) pore topology, and HZSM-5. Pt-Sn/SAPO-34 showed improved performance with propylene selectivity > 94% and 23% yield, whereas PtSn/HZSM-5 displayed high conversion but low selectivity to propylene (about 40 wt%) due to strong BrØnsted acidity and its large pore sizes, which favor cracking. The high activity of HZSM-5 was attributed to high surface acidity, which makes it active for propane dehydrogenation. Deactivation of HZSM-5 was more than 30% greater than SAPO-34 for the ODPC reaction. In addition, regeneration of HZSM-5 supported catalyst led to dealumination because its structure is aluminum-based while SAPO-34 is hydrothermally stable and its structure is Si-based with pore size comparable to propylene, favoring selectivity. In another study, Nawaz et al. [99] found that the concentration of Pt active sites was higher at the calcination temperature of 500 °C, which they indicated has superior activity. However, with calcination at 400 °C, directly anchored Pt sites increased, while with a calcination at 600 °C, metal sintering and reduction in Pt-Sn and Sn-support interactions resulted in lower dehydrogenation activity. Propane dehydrogenation over various SAPO-34 supported metal catalysts is listed in Table 3.

Recently, Kim et al. [100] grew micrometer-thin SAPO-34 zeolite membranes on α-alumina tubular supports and used them for propane dehydrogenation reaction at 600 °C. Propylene selectivities greater than 80% and propane conversions of 65–75% at weight hourly space velocities of 0.1–0.5 h^{-1} were reported (Fig. 10). The efficient removal of produced hydrogen in the ODP reaction by the membranes was responsible for the high performance.

It is generally believed that the access to active sites of zeolites differs considerably due to various crystal structures but this class of porous materials can also be used as metal oxide supports in development of bifunctional catalysts (metals and zeolite composite) for ODPC reaction. In order to avoid side reactions, the acidity and oxidizing ability of the bifunctional catalysts should be optimized. The motivation for replacing aluminum in MFI or CHA zeolite structures by other elements arose from the need to adjust acid-base and redox properties to intended applications as well as mechanical properties, however, this type of composite materials have not been studied in detail for ODPC reaction. Furthermore, the dynamics of non-framework species under reaction conditions that involve redox process, adsorption of reactants/products, and electrical conductivity variations, that are affecting the reaction mechanism and subsequently the way they contribute to catalytic reactions are not yet fully understood. With the ability to fine-tune the structural, topological, and surface properties, the zeolitic materials appear to offer a great opportunity for developing advanced bifunctional materials that overcome the problems of current materials and show high activity and stability in the ODPC reaction. Indeed, this should be considered as one of the central issues of future research in this field.

Table 3
Propane dehydrogenation over metal supported SAPO-34 structure in the absence of CO_2.

Catalyst	Si/Al	S_{BET} m^2/g	Feed, H_2/C_3H_8	WHSV h^{-1}	TOS h	XC_3H_8 %	$S_{C_3}H_6$ %	$Y_{C_3}H_6$ %	Refs.
SAPO-34	–	441	0.25	5.6	4	3	38	1.14	[92]
Pt/SAPO-34	–	424	0.25	5.6	4	12	87	10.44	[92]
Pt-Sn/SAPO-34	–	419	0.25	5.6	4	19	94	17.86	[92]
Pt-Sn/HZSM-5	140	396	0.25	5.6	4	25	40	10	[92]
Pt-Sn/SAPO-34[a]	–	412	0.25	5.6	4	14	88	12.32	[99]
Pt-Sn/SAPO-34[b]	–	409	0.25	5.6	4	18	92	16.56	[99]
Pt-Sn/SAPO-34[c]	–	391	0.25	5.6	4	13	72	9.36	[99]

[a] = calcination temperature of 400 °C.
[b] = 500 °C.
[c] = 600 °C.

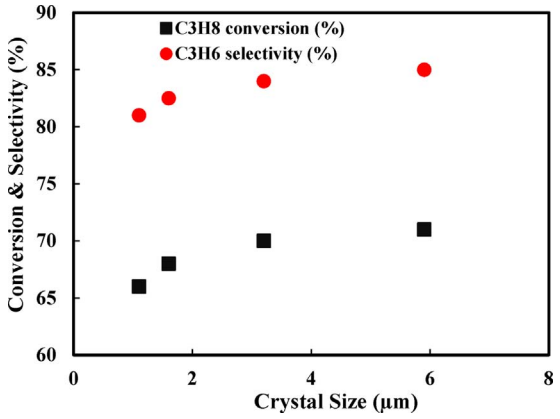

Fig. 10. Dehydrogenation of propane to propylene over SAPO-34/α-alumina tubular supports [100].

4.2. Oxidative dehydrogenation of propane with CO_2 over metal oxide-based catalysts

To date, several metal oxides such as CrO_x, VO_x, FeO_x, MoO_x, GaO_x, and InO_x deposited on the surface of various mesoporous and/or microporous supports including SiO_2, Al_2O_3, TiO_2, ZrO_2, CeO, NbO_5, MgO, zeolites, and carboneous materials have been most frequently reported as dehydrogenation catalysts for paraffinic C—H bond activation [29,36,38,101–116]. The relatively high catalytic activity of transition metal oxides is attributed to their reducible nature and their ability to easily change their oxidation state. Apart from structural and physicochemical properties, the method in which the metal oxide is deposited onto a support and metal-support interaction can have significant influence on the performance of the final catalyst in the ODH of light alkanes. In the following sections, we will review the catalytic behavior of chromium-, vanadium-, gallium-, and indium-based oxide catalysts in OPDC reaction.

4.2.1. Chromium-based catalysts

It is a broad consensus that the ODP reaction over chromium-based catalysts follows the Mars-Van Krevelen mechanism [38,112,113]. During this phase of the reaction process, Cr^{6+} reduces to Cr^{3+} or Cr^{2+} species that are responsible for the ODH reaction [33,117]. The fraction of the reducible species depends primarily on the support type, coverage level and chromium dispersion [90]. At a low Cr content, where a high dispersion is expected, migration of Cr^{3+} species to stable Cr_2O_3 clusters is slow, therefore Cr^{3+} may be further reduced to Cr^{2+} [117]. However, the dispersion is lower at a high Cr content, therefore the reduction stops at Cr_2O_3 [117]. Shishido and his colleagues [36] used Cr K-edge XAFS spectra and TPR profiles to confirm that the redox cycle between Cr^{6+} and $Cr(VI)O_4$ has an important role in the dehydrogenation of C_3H_8 over both Cr/SiO_2 and Cr/Al_2O_3 catalysts, regardless of the support. According to their study, CO_2 oxidizes a part of Cr^{3+} to Cr^{6+} species under the reaction conditions. As a result, in the case of Cr/SiO_2, the oxidative dehydrogenation of C_3H_8 over Cr^{6+} species takes place in addition to the simple dehydrogenation over Cr^{3+} species. Fig. 11 shows the proposed mechanism for dehydrogenation over chromium-based catalysts. The Cr^{6+} species was found to be crucial for high activity in the ODPC reaction. The rate of propylene formation increased almost proportionally with the concentration of Cr^{6+} species in the calcined catalysts. According to this mechanism, at the beginning of the ODP reaction, the reduction of Cr^{6+} species generates dispersed Cr^{3+} and Cr^{2+} sites that participate in non-oxidative pathway of propylene formation. In the presence of CO_2, Cr^{3+} and Cr^{2+} sites may participate additionally in an alternative oxidative pathway of propylene formation and in a consumption of hydrogen produced in the ODP by RWGS reaction.

Wu et al. [33] recently investigated a series of Cr_2O_3–ZrO_2 mixed oxides prepared by the hydrothermal method at 180 °C for ODPC reaction. The reaction was carried out at 550 °C with 2.5 vol% C_3H_8, 5 vol % CO_2, and a balance of N_2. The catalyst prepared from a hydrothermal treatment gave rise to an initial propane conversion of 53.3%, which was 1.6 times that of the conventional Cr_2O_3-ZrO_2. The enhanced activity of the hydrothermally prepared catalysts was attributed to higher surface area and higher concentration of Cr^{6+} than Cr^{3+} since Cr^{6+} species are more active in the reaction. In the absence of CO_2, conversion of 76.5%, selectivity of 60.3%, and turn over frequency (TOF) of $14.8 \times 10^4\ s^{-1}$ were obtained within 10 min, but both conversion and TOF values quickly dropped to 3% and $0.6 \times 10^4\ s^{-1}$, respectively, while selectivity reached 97.4% within 6 h reaction time with 9 wt% coke deposition. In the presence of CO_2 however, the same behavior was observed in which initial conversion and TOF experienced a dropped from 53.3% and $10.3 \times 10^4\ s^{-1}$ to 27.7% and $5.4 \times 10^4\ s^{-1}$ respectively, while selectivity showed an enhancement from 79% to 90.8% in the same 6 h reaction time 2.7 wt% coking [33]. The lower initial conversion of C_3H_8 in the presence of CO_2 was correlated to competitive adsorption of CO_2 and C_3H_8 on the catalyst. Moreover, the enhanced catalyst stability was associated to a decreased amount of carbon deposited on the catalyst surface according to the reverse Bourdard reaction.

Agafonov et al. [112] studied the effect of synthesis conditions (*e.g.* solution pH, support calcination, and Cr loading) on the activity of CrO_x/SiO_2 catalysts for ODPC reaction. It was shown that changes in preparation procedure dramatically affects the activity and stability of the catalysts in the ODPC reaction. The catalytic test was carried out at 1 atm, 600 °C, and a space velocity of $200\ h^{-1}$ using a feed composition of C_3H_8:CO_2:N_2 = 15:30:55, vol%. As Fig. 12a demonstrates, the

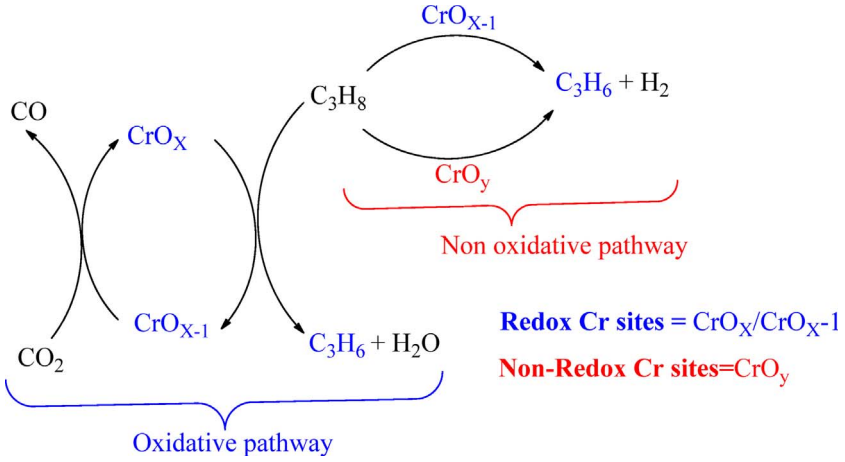

Fig. 11. Possible reaction mechanism of ODPC on chromium-based catalysts [26,36,54].

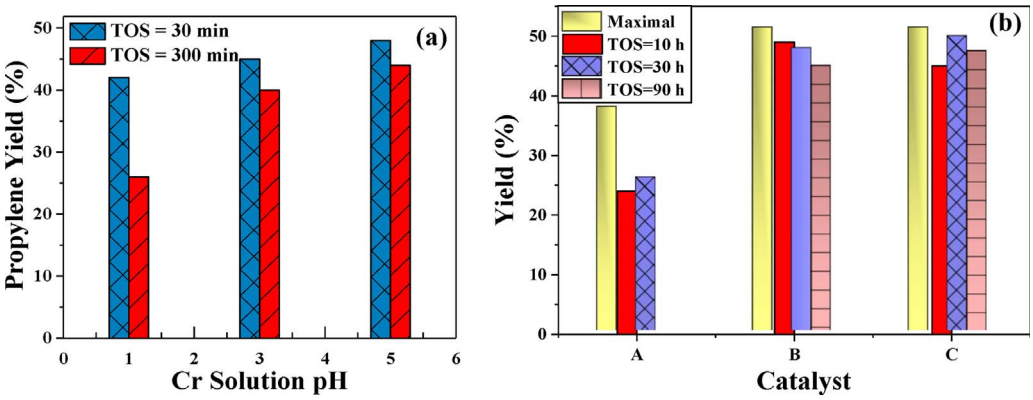

Fig. 12. Yield of propylene in the ODPC reaction (a) as a function of Cr solution pH, and (b) over the 5 wt% CrO_x/SiO_2 of series A-C (A: non-calcined silica support, B: calcined silica support, C: heated to 600 °C and calcined silica support) [112].

propylene yield varied with the chromium solution pH, exhibiting enhanced catalytic activity and stability up to pH of 5 while beyond this value, the precipitation of chromium hydroxide took place. Generally, the acidity increases the number of sites responsible for adsorption and polymerization of olefins. CrO_x/SiO_2 catalysts are well-established polymerization catalysts and increasing acidity favors the formation of CrO particles on the support surface. CrO easily reduces to low oxidation states during dehydrogenation. Moreover, the authors prepared different series of catalysts (A, B, C) and showed that calcination of the support makes it possible to attain a more uniform distribution of active phases on the surface, hence a higher propylene yield, as illustrated in Fig. 12b. It was also shown that the catalytic activity of Cr increased with increased Cr loading, reaching a maximum at 5 wt%. Above 5 wt% loading, significant decrease in activity of the catalysts was observed for ODPC reaction.

In another investigation, Botavina and coworkers [39] reported encouraging results at 5 wt% loading of Cr on SiO_2, but the catalyst deactivated quickly due to agglomeration of chromium species. In a later study [27], the same authors used direct hydrothermal synthesis to improve the dispersion of chromium species on the support for ODP reaction in CO_2 or CO_2 + O_2 environment under conditions close to industrial conditions. The initial C_3H_8 conversion in ODP with CO_2 as the oxidant increased from ca. 40% for 0.25-Cr/SiO_2 to a maximum ca. 70% at 2.0 wt% Cr/SiO_2 and remained at 50% after 6 h for 2.0 wt% Cr/SiO_2. Thermodynamic calculations indicated that the equilibrium conversion of ODPC reaction (Eq. (3)) at 873 K is 67%. As a result of the different mechanisms and other possible simultaneous beneficial effects, the initial C_3H_8 conversion values obtained for the ODP in the presence of CO_2, O_2, or CO_2 + O_2 were 70, 75, and 80%, respectively, which decreased to 50, 65, and 70% after 900 min of reaction. When the catalyst was tested under non-oxidative conditions, the initial conversion was low at 60% and dropped to 40% within 6 h TOS. In addition, propane yield of 47% was attained over 2.0 wt% Cr/SiO_2 when CO_2 was used as the oxidant and remained up to 40% after 1000 min (among the highest reported so far). For ODP with O_2 + CO_2 as oxidant, C_2H_4 was found to be the main product after 300 min TOS due to enhanced cracking of propane in the presence of O_2, which was also responsible for the production of a larger excess of CH_4. The authors therefore suggested investigating the possibility of tuning the O_2/CO_2 ratio in order to obtain a desired composition of the olefin mixture for applications in C_2H_4/C_3H_6 copolymerization processes [27,112].

In summary, catalytic performance of chromium-based catalysts is drastically affected by the synthesis method, nature of the support, structure of the catalyst, nature of promoter-support interaction, active sites present in the catalyst, and the reaction conditions. To this effect, different authors have reported different chromium catalytic systems for ODPC reaction. Although chromium-based catalysts have exhibited promising results, however, due to potential environmental and health risks associated with the use of chromium, alternative catalysts should be designed and developed to enable a more sustainable process technology.

4.2.2. *Vanadium-based oxide catalysts*

Vanadium-based materials are one of the most active, selective, and well investigated catalysts for the ODH of light alkanes [8,31,101,118,119]. Supported vanadium oxide catalysts have typically been found to be more selective than the unsupported bulk V_2O_5 mainly because of the interactions of VO*x* species with the oxide supports (*e.g.* Al_2O_3, Nb_2O_5, TiO_2, ZrO_2, SiO_2, *etc.*) [116,119,120]. It has been reported that the interaction between the oxide support and the deposited vanadium oxide determines the structure of the resulting surface VO*x* species [6,109,114]. Dehydrated surface VO*x* species have been found to possess VO_4 coordination with one terminal V═O bond and varying degrees of polymerization on different supports [105,110]. At high-surface vanadium oxide coverage, crystalline V_2O_5 nanoparticles also exist. This bulky vanadium pentoxide demonstrates a relatively low catalytic performance for selective alkane oxidation [8,102,111,121]. The catalytic activity of vanadium in ODP and the propylene selectivity are considered to be a function of the ratio of different vanadium oxide species, loading, calcination temperature, additives, and the specific support used. The factors that govern the catalytic performance of the surface VO*x* species, however, are still being debated [6,30,121].

The reaction of both supported and unsupported vanadium catalysts follow the Mars-Van Krevelen redox mechanism involving lattice oxygen in C—H bond activation and that each reaction turnover requires a two-electron reduction of high-valent M^{+n} cations to form one M^{n-2} or two M^{n-1} cations [8,38,119]. This is the kinetically relevant step for both ODP and combustion reactions involving the activation of methylene C—H bonds in propane [8,36,38]. The alkyl species produced desorb as propylene and the remaining hydroxyl (OH) groups recombine with neighboring groups to form water molecules and reduced vanadium centers [8]. The addition of CO_2 could promote desorption of the water formed. The reduced vanadium centers can be re-oxidized by dissociative chemisorption of O_2 [38]. On VO*x*- and MoO*x*-based catalysts, the rate constants for re-oxidation of reduced centers using O_2 are greater than that for their re-reduction by C—H bond activation steps [36]. Some researchers have proposed that ODP rates increase as active metal oxides become more reducible [15,36,119,122]. The main reactive intermediates during ODP reaction over VO_x domains are surface oxygen, O—H groups, and oxygen vacancies [39]. Iglesia et al. [119] have explored the electron transfer processes required for C—H bond activation steps and the factors responsible for the redox processes involved in each propane turnover. In that work, ODP turnover rates were reported on active oxides (VO_x, MoO_x, NbO_x, and WO*x*) that were dispersed as isolated or two-dimensional species on the surface of inactive Al_2O_3, ZrO_2, or MgO supports. Their findings showed that both turnover rates and H_2-reduction rates increase with increasing MO_x (where M = metal) surface density, as indicated in Fig. 13.

Du et al. [123] also explained that the methylene C—H bonds in a propane molecule are weaker than the methyl bonds. These weaker bonds first interact with lattice oxygen as a propane molecule adsorbs

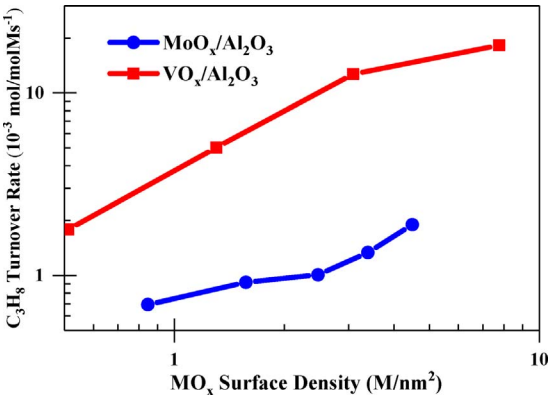

Fig. 13. Dependence of propane turnover rate on the MO_x surface density (703 K, 14 kPa C_3H_8, 1.7 kPa O_2, balance He) [119].

weakly on the oxide surface [119,123,124]. The adsorbed propane reacts with a vicinal lattice oxygen atom to form an isopropoxide species and an OH group [119,125].

Zhang et al. [87] examined a series of V-Cr/SBA-15/Al_2O_3/FeCrAl metal monolithic catalysts with V content of 10 wt% and Cr contents from 0 to 12.5 wt% for ODPC reaction. The catalysts were tested in a fixed-bed reactor at 1 atm, 450–700 °C,C_3H_8/CO_2 space velocity of GHSV = 14400 ml/g h, and V_{CO2}/V_{C3H8} molar ratio of 3. Using XPS analysis, it was confirmed that the oxidation states of V were +5 and +4. With the addition of Cr species, the relative content and total amount of V^{5+} species increased and reached a maximum at 10 wt% Cr content. By further increase in Cr content to 12.5%, the relative content of V^{5+} species dropped remarebly. This was attributed to the formation of more Cr^{3+} species that hamper the formation of dispersed tetrahedral V^{5+} species. Similarly, Cr^{3+} and Cr^{6+} species were present in the catalysts and the amount of Cr^{6+} increased to a maximum at 10 wt % Cr. The V-Cr/SBA-15/Al_2O_3/FeCrAl catalyst with 10 wt% V and 10 wt% Cr exhibited the best activity with a propane conversion of 49.9%, propylene selectivity of 86.5% and a yield of 42.5% at 650 °C. Above these loadings, the yield of propylene decreased and the selectivity to minor products such as methane and ethane increased. The tetrahedral vanadium (V^{5+}) species were the main active species in the ODP reaction. The strong interaction between vanadium oxide and chromium oxide was believed to be accounted for changing the redox properties and enhancing the catalytic activity of the catalysts [87].

Moreover, hydrogenolysis reactions (Eqs. (8)–(9)) are typically promoted by low coordination site defects such as Steps and Kinks [126,127]. These side reactions can be hindered by using nano-size materials in the case of Pt-based catalysts. Jibril and his colleagues [126] employed the synergistic effect of promoter, support, and additives, and the influence of nano-size catalysts to test VMgO-based nanowires ($Mg0.15\,V_2O_5\cdot 2{\cdot}4H_2O$) mechanically mixed with either Al_2O_3 or SiO_2 for the ODP reaction. The catalyst was prepared by the aqueous method and tested at 500, 550 and 600 °C with gas flow of 70 cm^3/min (C_3H_8:Ar ratio of 2:5) at 1 atm. The active species were V_2O_5 and MgV_2O_6, resulting from decomposition of layered nanowires of $Mg0.15\,V_2O_5\cdot 2{\cdot}4H_2O$ at high temperature. Their results indicated that both supports enhance the conversion and selectivity to propylene, however, Al_2O_3 support performed much better with higher conversion and selectivity compared to SiO_2. The better performance of Al_2O_3 support is explained to be caused by a higher rate of propylene desorption, whereas on the SiO_2 surface, there is high electrophilic attack on propylene, thereby reducing its selectivity.

Typically, selectivity is enhanced by the presence of sites that remove hydrogen. Further removal of hydrogen leads to olefins or cracking products. After hydrogen is produced, the rate of desorption is important. Otherwise, it combines with alkenes and/or alkyl species to produce alkanes [126,128]. Cracking reaction results in lower alkanes, hydrogen, and carbon deposits [126,128,129].

In continuation of the search for higher performing vanadium catalysts, Kootenaei et al. [121] investigated vanadia loading and calcination temperature effects on morphology and catalytic performance of vanadia supported on titanate nanostructures in ODPC reaction. The wet impregnation method was used to prepare 5 wt% V_2O_5 supported on TiO_2 and VTNT-x (x wt% V_2O_5 supported on titanate nanotube) and tested in a fixed-bed reactor at 500 °C and 1 atm using equal flows of air and propane with total flow rate of 100 mL min^{-1}. The BET surface area of TiO_2 support was higher in the case of nanotubes. The molecular structures of supported vanadia catalysts under dehydrated conditions transformed from monodispersed vanadia species to polyvanadate species as vanadia loading increased. Higher loadings above monolayer coverage of support led to a tendency to develop a crystalline phase [121,130]. It has been reported that complete coverage of the support surface with vanadium oxide is established with 4.98×10^{14} molecules of V_2O_5 cm^{-2} [121]. Besides propylene, H_2O, CO, and CO_2 were recorded as products with CH_4 and C_2H_6 appearing at high temperatures. Relatively higher conversions and TOF values were obtained for titanium nanotubes compared to titanium oxide with similar loadings. The lower performance of the oxide is due to the rutile phase titanium oxide, while anatase polymorph of titanium accounted for higher conversions in the nanotubes. Titanium oxide normally exists as rutile and anatase polymorphs. However, the anatase is usually unstable and easily converts to the stable rutile phase with an accompanied loss in surface area [121,131]. This irreversible phase transition is the major cause of deactivation in titanium-based catalysts. This transformation is influenced by particle size, rutile content, surface area, calcination temperature and time, atmosphere, additives and impurities, and redox cycle [121,132].

In summary, the performance of the active components in a vanadium-based catalyst has been shown to depend primarily on the type of support/template and promoter that affect catalyst redox and surface acidic properties. Due to susceptibility of the electron-rich centers to ODPC reaction, acidic sites promote cracking of olefins products or propyl species and formation of coke. Moreover, the nano-size particles tend to exhibit higher catalytic activity and selectivity than the bulk catalyst, implying that propane molecules have a greater chance to interact with active sites that abstract hydrogen. Thus, the design strategy should take into consideration all these factors simultaneously for improving the performance of vanadium catalysts. The future prospects of vanadium-based catalysts is bright, and there is a potential in ODPC industry to market the utilization of CO_2 as a soft oxidant over this class of materials.

4.2.3. Gallium and indium-based oxide catalysts

Gallium-based catalysts became a subject of investigation after Nakagawa reported exceptional activity of commercial Ga_2O_3 catalysts for ethane dehydrogenation to ethylene in the presence of CO_2 [31,133]. Studies have shown that Ga_2O_3 can be active and stable in the ODH of light alkanes, and outperform Cr_2O_3 and V_2O_5 catalysts [31,133]. It has been proven that the activity of gallium-based catalysts is dictated by the coordination state and reducibility of gallium species, nature of the support, acid-base properties, and gallium content [84,133–135]. Typically, activities correlate positively with medium–-strong acidity (BrØnsted acidity). However, in the case of $Ga_xAl_{10-x}O_{15}$ oxides, activities correspond with weak (Lewis) acidity [64,133]. Since tetrahedrally coordinated Ga^{3+} species are responsible for Lewis acidity, they are assumed as central components for the ODP reaction [133]. Sattler et al. [84] made similar analyses in which unsaturated Ga^{3+} species were deemed responsible for C—H bond activation. In their study, Pt was used as an additive to kindle the distribution and tetrahedral coordination of Ga^{3+} species on the surface of the catalyst and help in the recombination of hydrogen adsorbed on the catalyst. Encouraging results have been achieved with Ga_2O_3 dispersed on inert supports such as TiO_2 and Al_2O_3 for ODP reaction at 500 °C [136,133]. Many different forms of gallium-based catalysts such as spinel-like

gallium solid solutions [133], ternary mixtures of Ga/In/Al [136], and polymorphs of gallium [134] have been investigated for ODP reaction. Chen et al. [133] synthesized a series of mixed $Ga_xAl_{10-x}O_{15}$ oxide (with x varying from 0 to 10) catalysts using the alcoholic co-precipitation method for propane dehydrogenation under different environments (CO_2 and without CO_2). Within this series of catalysts, the maximum activity was reported for $x = 8$ while the highest stability was achieved for Ga_2O_3–Al_2O_3 with higher aluminum content. Moreover, linking the activities with the NH_3-TPD profiles, it was disclosed that high population of surface acid sites is connected to tetrahedral Ga^{3+} cations (responsible for Lewis acidity). The fraction of Ga^{3+} ions found in tetrahedral sites increased inversely with Ga/Al ratio, signifying that the Ga^{3+} ions preferentially occupied the tetrahedral sites of the defect spinel structure of the γ-Ga_2O_3–Al_2O_3 solid solution [133].

The thermodynamics of the propane dehydrogenation reaction designates that extent of reaction can be improved by coupling it with the RWGS reaction [37]. However, for some gallium-based catalysts, CO_2 does not stimulate all the catalysts for propane dehydrogenation due to the decrease in propane adsorption [32,133]. For instance, for $Ga_2Al_8O_{15}$ catalyst, the conversion was shown to decrease quickly with time in the presence of CO_2, whereas enhanced catalyst stability with relatively higher conversions with time were reported for γ-Ga_2O_3, $Ga_8Al_2O_{15}$, and $Ga_5Al_5O_{15}$. This boost to stability is suggested to be influenced by CO_2. Meanwhile, for $Ga_2Al_8O_{15}$, the poor catalytic performance was attributed to competitive adsorption between propane and CO_2 [133]. Michorczyk and Ogonowski [32] further reported propane conversion of 92% at 873 K (50 K lower than without CO_2) and CO_2/C_3H_8 molar ratio of 5 when the reaction was performed over Ga_2O_3 catalysts.

Chen's group [133] observed that for simple γ-Ga_2O_3 catalyst, the activity in the presence of CO_2 retards quickly from 33.7% to 2.1% within 16 h. On the other hand, $Ga_5Al_5O_{15}$ activity retardation was much slower, losing only 2.4% (from 33.7 to 26.5%) in 16 h. Conversion as high as 22.5% after 50 h TOS was reported. Quick deactivation with time in both the presence and absence of CO_2 was linked to catalyst coking [133]. Michorczyk et al. [64] clarified that the carbon deposition is associated with unsaturated hydrocarbons (olefins) and not saturated hydrocarbons (alkanes), and results from substrate–product reactivity. This explains the chemistry behind the higher coke deposition associated with higher conversion. By pulse reaction study, it was found that desorption of propylene from the catalyst surface was conducive on gallia–alumina mixed oxide catalyst surfaces and that accounted for the higher stability of those catalysts [84,133].

Sattler et al. [137] synthesized a stable catalyst that was more resistant to deactivation by depositing 1000 ppm Pt, 1.5% or 3 wt% Ga, and 0.25 wt% K on an alumina support. The catalyst were tested in ODPC reaction for eight successive dehydrogenation–regeneration cycles with 15 min dehydrogenation at 620 °C and 30 min regeneration at 750 °C in air. By combining Pt and Ga, conversions of 42% (close to the equilibrium conversion of 55% at 620 °C and 1 atm) and selectivity of about 96% were achieved. It was also reported that adding additives of alkali metals like K enhances the selectivity and reduces coking by poisoning the acid sites. Catalyst stability of 14 days at 31.1% conversion and 92.6% selectivity was established. The synergy between Ga and Pt species overrode the usual sintering deactivation associated with Pt catalysts. Using Operando Raman spectra study, it was confirmed that Pt only hydrogenates the carbon deposits, thereby improving the life of the catalysts while Ga does the actual dehydrogenation reaction [133].

In another investigation, Xu et al. [56] investigated the performance of a series of supported gallium oxide catalysts in ODPC reaction. As shown in Fig. 14, CO_2 promoted the catalytic dehydrogenation activity of Ga_2O_3/TiO_2 but suppressed those of Ga_2O_3/ZrO_2 and Ga_2O_3/Al_2O_3. Propane conversions of 32, 26, and 30% were obtained over Ga_2O_3/TiO_2, Ga_2O_3/Al_2O_3, and Ga_2O_3/ZrO_2 catalysts, respectively. Through XPS analysis of the catalysts, the authors hypothesized that the different

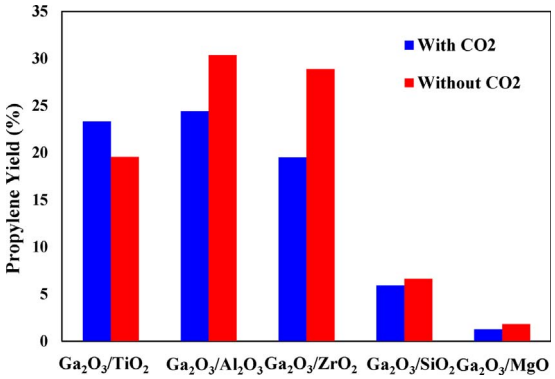

Fig. 14. Effect of TiO_2, Al_2O_3, ZrO_2, SiO_2 and MgO-supported Ga_2O_3 on propylene yield in the ODPC and ODP reactions [56].

behavior of the five supported Ga_2O_3 catalysts may stem from the difference in interactions between the support and the Ga_2O_3 species. However, through H_2 and propane pulse chemisorption tests, it was pointed out that two antagonistic roles of CO_2 exist in the reaction; the constructive role which is achieved by removing dissociatively adsorbed H_2 from catalyst surface by the RWGS reaction, and the damaging role which is achieved by displacing adsorbed propane on basic sites of catalyst.

Recently, Michorczyk et al. [64] carried out ODPC reaction over thermally stable mesoporous Ga_2O_3 and Ga_2O_3-Al_2O_3 oxides prepared by nanocasting method. Mesoporous Ga_2O_3 catalysts with large specific surface areas (231–322 m^2g^{-1}), uniform mesopores (3–14 nm), and pore architecture similar to that of SBA-15 (hexagonal structure) were obtained with this synthesis approach. It was further confirmed that high surface gallium species associated with Lewis acidity were responsible for higher conversions while the amount of coke deposited increased with the gallium species intensity. Mesoporous Ga_2O_3 showed better selectivity (91–95%) than Ga_2O_3-Al_2O_3 (85–92%) as a result of uniform mesopore structure and pore size distribution. The conversion of propane was almost low and constant (at 8%) for catalysts with Al_2O_3 support, implying that the support does not have much effect in conversions. It has been established that the selectivity to propylene in ODPC reaction over gallium is influenced by two factors; the acidity of the catalyst which is dependent on Ga_2O_3 phase composition or characteristics of support [56,84,134], and pore geometry of the catalysts [84]. Higher propylene selectivity was attained by α- and β-Ga_2O_3 than with δ- and γ-Ga_2O_3 phase catalysts [138].

In the same investigation [64], it was reported that higher temperatures promotes hydrocracking, cracking and dehydrocyclization, leading to production of light alkanes (methane and ethane), toluene, and benzene. The usual reverse Boudouard reaction that would normally occur in the presence of CO_2 did not take place at high reaction temperatures. Xu et al. [56] studied gallium supported on a series of metal oxide catalysts such as ZrO_2, TiO_2, SiO_2, Al_2O_3, SiO_2 and MgO for ODPC reaction. Their observations follow the heterolytic dissociative mechanism and the authors proposed the following steps (Eqs. (10)–(15)) in ODPC reaction over Ga_2O_3 catalyst.

$$C_3H_7{}^+S \rightleftharpoons C_3H_6 + S \quad (14)$$

It was found that the major pathway of the removal of the dissociatively adsorbed H_2 depends on the relative rate of steps 12 and 15 [56]. Liu et al. [139] studied the mechanism of propane activation over Ga (100) using DFT calculations. From their study, it was found that initial activation of C—H bond can occur in two ways: heterolytic dissociation mechanism (Eqs. (16) and (17)), where the acid-base pairs (Ga—O) polarize and then break the C—H bond, and homolytic dissociation mechanism (Eqs. (18) and (19)), where active site pairs consist of two O or Ga active sites and the C—H bond is polarized and activated by O or Ga sites.

$C_3H_8 + O\text{-}Ga \rightarrow OH + C_3H_7Ga$ (16)

$C_3H_8 + Ga\text{-}O \rightarrow GaH + C_3H_7O$ (17)

$C_3H_8 + O\text{-}O \rightarrow OH + C_3H_7O$ (18)

$C_3H_8 + Ga\text{-}Ga \rightarrow GaH + C_3H_7Ga$ (19)

The above reactions could also be explained in terms of propylene formation. One pathway is H abstraction from physically adsorbed propyl radical (Eq. (16)), and the other is H abstraction from propoxide (Eqs. (17) and (18)) or propylgallium intermediates (Eq. (19)). For both pathways, propylene formation on O(2) sites has lower energy barrier. On the other hand, surface hydroxyl groups formed are stable since formation of either H_2 or H_2O from them is difficult. Also, propylene adsorbed on these hydroxyl groups is difficult to desorb and prone to further dehydrogenation or oligomerization. As a consequence, catalytic activity decreases quickly when surface oxygen sites are covered by hydrogen and the surface is partially reduced. Furthermore, it was found that gallium sites are less active than oxygen sites, thus hydrogen abstraction would more often occur on oxygen sites. Nonetheless, when the surface oxygen sites are consumed, H abstraction from various propyl intermediates would occur on Ga sites to form propylene. Even though H abstraction by Ga has to overcome high energy barriers, the formation of H_2 from GaH and O(2)H or O(3)H hydroxyl groups is much easier than the formation of H_2 or H_2O from GaH or hydroxyl groups, implying a change in rate-determining step from H abstraction by oxygen sites at the initial stage of reaction to H abstraction by Ga sites to form GaH species [32,124,135]. Thus, applying oxidants like CO_2 and steam would remove the surface covering hydrogen and coke deposit, and suppress the equilibrium to form gaseous H_2O [139]. Contrary to the finding from theoretical DFT calculations, by using the MAS NMR study of propane interaction with Ga_2O_3 supported on zeolite, Gabrienko et al. [140] showed that the interaction of small alkanes with Ga_2O_3 or Ga-modified zeolite results in dissociative adsorption of alkane forming Ga-alkyl intermediate species rather than the alkoxy species.

Besides Cr-, V- and Ga-based materials, In_2O_3-basded catalysts have also demonstrated auspicious catalytic performance in ODP reaction [14,141]. Like gallium-based analogues, dehydrogenation reaction over indium-based catalysts in the presence of CO_2 follow a two-step process; the non-oxidative dehydrogenation of propane (Eq. (1)) followed by the RWGS reaction (Eq. (2)) [14,141]. However, unlike gallium-based catalysts which have been shown to have poor redox properties [133,137], indium-based materials exhibit good redox characteristics with highly dispersed and bulk In_2O_3 reducing from In^{3+} to In^0 [14,142]. Nevertheless, the reduced In^0 (active centers for dehydrogenation) species cannot be re-oxidized by CO_2 [14]. Indium reduced at low temperatures is associated with α-phase, whereas high temperature reduction is associated with β-phase [142]. The amount of dispersed In_2O_3 species was found to be dependent on the type of support in the order of In/Al > In/Zr > > In/Si. The period of indium reduction (lasting 3 h), normally called the induction period, is accompanied by low conversions and selectivies, after which improved conversion and selectivities are obtained [141], suggesting the reduced metallic In^0 are the active species, unlike gallium-based catalysts in which Ga^{3+} are the active species. The reduced indium species are thought to have come from highly dispersed In_2O_3, thus designing a catalyst that can effectively disperse indium promoter may be a key factor in achieving higher performance. For high indium loadings on SiO_2 support, the induction period does not take place. This was suggested to be due to overpopulation of In_2O_3, probably resulting from less interaction of In_2O_3 with the silica support [14].

Chen et al. [141] demonstrated that a bifunctional In_2O_3–Al_2O_3 catalyst is more stable and active, with indium species and In_2O_3 playing a major role in In_2O_3–Al_2O_3 system's activity for CO_2-incorporated reactions (Fig. 15). In that study, a series of catalysts were

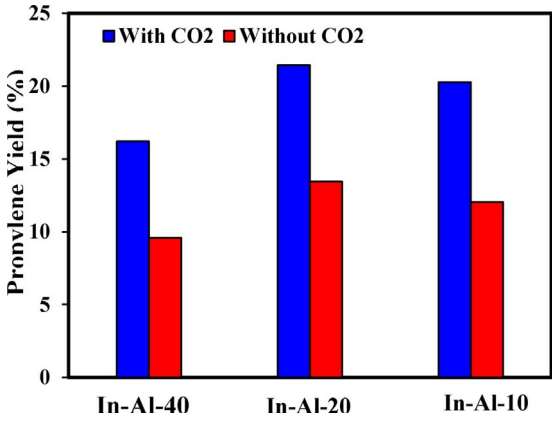

Fig. 15. Effect of bifunctional In_2O_3-Al_2O_3 catalyst with various loading on ODPC and ODP reactions [141].

prepared with different indium promoter loadings on Al_2O_3, ZrO_2, and SiO_2 supports using the wet impregnation method, and the acid-base properties of the supports and their interactions with In_2O_3 were examined for ODPC reaction. On the issue of acidity, indium indicated a divergent effect on acidity, whereas the support paralleled the degree of acidity in the order of ZrO_2 > Al_2O_3 > SiO_2 [14]. On the contrary, both promoter and support showed positive synergy in basicity of the catalysts.

Catalytic activities positively correlate with the amount of In^0 species and the acidity on the surface of the catalysts. The yield of propane were in the order of In/Zr > In/Al > In/Si, testifying to the importance of the support acidity effect. Without CO_2 however, the catalytic activity varied, with In_2O_3-Al_2O_3 displaying the best performance. This change in catalytic activity could imply that the support has an effect on the RWGS reaction, which is important for breaking the thermodynamic equilibrium barrier. Generally, acidic gases would adsorb onto basic sites, thus the high basicity of In_2O_3-ZrO_2 catalysts could account for their superior performance in the presence of CO_2.

Despite the fact that acidity is necessary for better catalytic performance, it is also known that acidity higher than optimum promotes side reactions and quick deactivation, leading to low selectivity to the desired product. Thus, to achieve selectively high conversion of propane for the supported In_2O_3 samples, well dispersion of In_2O_3 and balanced acid-base properties are crucial rudiments. Furthermore, it has been suggested that the acid-base properties and the abundance of surface dispersed indium species are responsible for propane dehydrogenation. The dispersion of the active species and electronic properties of dispersed active species are influenced by the type of support. These together with the acid-base properties of the support affect the selectivity to propylene. Therefore, indium will be one of the suitable elements to use as dopant for engineering the catalysts properties. The ODP reaction parameters for metal oxide catalysts in the presence and absence of CO_2 are given in Tables 4 and 5, respectively.

In summary, the conversion of propane to propylene in the presence of CO_2 involves simultaneous occurrence of both non-oxidative dehydrogenation and oxidative dehydrogenation pathways, depending on whether the metal is reduced or not and/or the nature of the active sites. In the presence of redox metal oxide catalysts (*e.g.* Cr, V, Fe, Mo *etc.*), the reaction is mostly through one-step oxidative route with CO_2 re-oxidizing the reduced metals (Eq. (3)) in concomitance with the Mars–Van Krevelen mechanism. Some of these redox catalysts were discussed above. However, in the case of non-redox catalysts (*e.g.* Ga, In), the reaction proceeds *via* two-step non-oxidative route. The first reaction is non-oxidative dehydrogenation (Eq. (1)) and the second is CO_2 participation in RWGS reaction (Eq. (2)) by removing the produced H_2 and shifting the equilibrium position towards higher conversions of propane. For catalysts that cannot be reduced at dehydrogenation

Table 4
Metal oxide catalysts for propane dehydrogenation in the presence of CO_2.

Catalyst	S_{BET} m^2/g	Feed C_3H_6:CO_2:N_2	W/F g min/mL	TOS h	T °C	XC_3H_8 %	$S_{C_3}H_6$ %	YC_3H_6 %	Refs.
Cr-MSU-x28	791	1:01:08	0.00667	2	400	1.62	97	2.2	[89]
Cr-MSU-x28	791	1:01:08	0.00667	2	500	12.1	94.8	11.4	[89]
Cr-MSU-x28	791	1:01:08	0.00667	1.5	600	36.8	90.4	35.5	[89]
Cr-MSU-x28	791	1:01:08	0.00667	1	700	78.5	60	44.2	[89]
Cr-MSU-x3	903	1:01:08	0.00667	2	600	15	83	12	[89]
Cr-MSU-x10	896	1:01:08	0.0067	2.1	600	20	88	18	[89]
Cr-MSU-x14	848	1:01:08	0.0067	2.1	600	27	82	22	[89]
Cr-MSU-x51	754	1:01:08	0.0067	2.1	600	30	90	26	[89]
Cr-MSU-x82	730	1:01:08	0.0067	2.1	600	24	86	20	[89]
CrO/SiO_2	–	C_3:CO_2 1:5	16.67	0.17	550	17.2	94.4	16.3	[37]
CrO/SiO_2	–	C_3:CO_2 1:5	16.67	0.17	600	27.7	90.8	25.2	[37]
CrO/Al_2O_3	–	C_3:CO_2 1:5	16.67	0.17	550	12.9	88.3	11.4	[37]
CrO/Al_2O_3	–	C_3:CO_2 1:5	16.67	0.17	600	29.9	80.7	24	[37]
Cr_2O_3/ZrO_2	123	2.5:5:92.5	0.01	6	550	12.7	94	11.9	[33]
Cr_2O_3/ZrO_2	154	2.5:5:92.5	0.01	6	500–600	19.8	93	18.4	[33]
Cr_2O_3/ZrO_2	194	2.5:5:92.5	0.01	6	500–600	6.5	91.7	5.	[33]
Cr_2O_3/ZrO_2	178	2.5:5:92.5	0.01	6	500–600	27.8	90.8	25.2	[33]
Cr_2O_3/ZrO_2	178	2.5:5:92.5	0.01	6	500–600	3	97.4	2.9	[33]
$1\%Cr/SiO_2$	314	15:30:55	200 h^{-1}	20	600	55	76.4	42	[112]
$2\%Cr/SiO_2$	312	15:30:55	200 h^{-1}	20	600	53	90.6	48	[112]
$3\%Cr/SiO_2$	310	15:30:55	200 h^{-1}	20	600	65	65.4	42.5	[112]
$5\%Cr/SiO_2$	307	15:30:55	200 h^{-1}	20	600	69	–	45	[112]
$7\%Cr/SiO_2$	272	15:30:55	200 h^{-1}	20	600	60	–	47	[112]
$0.25\%Cr_2O_3/SiO_2$	960	15:30:55	200 h^{-1}	16.67	600	28	81	31	[27]
$0.5\%Cr_2O_3/SiO_2$	957	15:30:55	200 h^{-1}	16.67	600	30	75	37	[27]
$1\%Cr_2O_3/SiO_2$	910	15:30:55	200 h^{-1}	16.67	600	37	73	45	[27]
$2\%Cr_2O_3/SiO_2$	663	15:30:55	200 h^{-1}	16.67	600	50	66	47	[27]
$0.5\%Cr_2O_3/SiO_2$	957	15:30:3:52	200 h^{-1}	16.67	600	70	53	37	[27]
$1\%Cr_2O_3/SiO_2$	910	15:30:3:52	200 h^{-1}	16.67	600	77	46	35	[27]
$2\%Cr_2O_3/SiO_2$	663	15:30:3:52	200 h^{-1}	16.67	600	82	43	35	[27]
ZrO_2	19	2.5:5:92.5	0.01	4	600	5.6	77.8	4.4	[143]
$5\%Ga/ZrO_2$	34.8	2.5:5:92.5	0.01	4	600	27.9	54.3	15.2	[143]
$10\%Ga/ZrO_2$	42	2.5:5:92.5	0.01	4	600	32.8	48	15.7	[143]
$15\%Ga/ZrO_2$	53.9	2.5:5:92.5	0.01	4	600	38.6	45.4	17.5	[143]
$20\%Ga/ZrO_2$	59.1	2.5:5:92.5	0.01	4	600	41.8	43.1	18	[143]
$68.2\%Ga_2O_3$-m	231	1:05:09	0.0067	3.75	500–600	16	94	17.5	[64]
$71.9\%Ga_2O_3$-t	44	2.5:5:92.5	0.0067	3.75	500–600	7	92	19.6	[64]
$45.9\%Ga_2O_3/Al_2O_3$	276	2.5:5:92.5	0.0067	3.75	500–600	17	95.5	17.4	[64]
$12.4\%Ga_2O_3/Al_2O_3$	322	2.5:5:92.5	0.0067	3.75	500–600	17	97	9.4	[64]
γ-Ga_2O_3	104	2.5: 5:92.5	0.02	8	500	17	98.2	16.7	[133]
$Ga_8Al_2O_{15}$	119	2.5: 5:92.5	0.02	8	500	33.1	98	32.4	[133]
$Ga_5Al_5O_{15}$	130	2.5: 5:92.5	0.02	8	500	28	97.1	27.2	[133]
$Ga_2Al_8O_{15}$	147	2.5: 5:92.5	0.02	8	500	18	95	17.1	[133]
Al_2O_3	173	2.5: 5:92.5	0.02	8	500	0.5	88.4	0.4	[133]
Ga_2O_3/TiO_2	47	2.5: 5:92.5	0.01	0.167	600	32	73	23.3	[56]
Ga_2O_3/Al_2O_3	102	2.5: 5:92.5	0.01	0.167	600	26	94	24.4	[56]
Ga_2O_3/ZrO_2	19	2.5: 5:92.5	0.02	0.167	500	30	65	19.5	[56]
Ga_2O_3/SiO_2	329	2.5: 5:92.5	0.02	0.167	500	6.4	92	5.9	[56]
Ga_2O_3/MgO	35	2.5: 5:92.5	0.02	0.167	500	4.3	29	1.3	[56]
In_2O_3	23	2.5:10:87.5	0.02	8	600	3.5	58	2.0	[14]
$3\%In_2O_3/Al_2O_3$	112	2.5:10:87.5	0.02	8	600	14.5	84	12.18	[14]
$10\%In_2O_3/Al_2O_3$	105	2.5:10:87.5	0.02	8	600	24	84	20.2	[14]
$3\%In_2O_3/ZrO_2$	34	2.5:10:87.5	0.02	8	600	23	60	13.8	[14]
$10\%In_2O_3/ZrO_2$	30	2.5:10:87.5	0.02	8	600	39	65	25.3	[14]
$3\%In_2O_3/Al_2O_3$	264	2.5:10:87.5	0.02	8	600	4.7	68	3.2	[14]
$3\%In_2O_3/Al_2O_3$	259	2.5:10:87.5	0.02	8	600	4.8	59	2.83	[14]
In-Al-40	94	2.5:10:87.5	0.02	12	500	22.5	72	16.2	[141]
In-Al-20	174	2.5:10:87.5	0.02	12	500	27.5	78	21.4	[141]
In-Al-10	195	2.5:10:87.5	0.02	12	500	26	78	20.3	[141]

(Inert in the feed composition represents Ar, He, or N_2; X = conversion; S = selectivity; Y = yield).

temperatures, the redox mechanism is not applicable and propane is heterolytically dissociatively adsorbed on metal oxide, forming metal hydride and metal alkoxy species. Therefore, in the development of metal-oxide materials with advanced catalytic performance for ODPC reaction, it is necessary to adjust their redox properties by judicious selection of promoters, supports, and additives. High thermally stable support with large surface area allows uniform distribution of reducible and active species on the surface, which further prevents aggregation and sintering of the catalyst particles and enhances the stability of the catalyst.

5. Effect of process conditions on ODPC reaction

Another important area of interest in every chemical process is the conditions under which the reaction occurs. A significant portion of expenditure in almost all chemical industries goes into the energy required for the process, which is normally tied to the temperatures and pressures under which the process occurs. This is not different from oxidative dehydrogenation reactions. It is in fact one of the barriers needed to differentiate it from non-oxidative dehydrogenation reactions of propane to propylene. In general, the rates of C—H and C—C cleavage

Table 5
Propane dehydrogenation over metal oxide catalysts in the absence of CO_2.

Catalyst	S_{BET} m^2/g	Feed vol%	W/F g min/mL	TOS h	T °C	XC_3H_8 %	$S_{C_3H_6}$ %	$Y_{C_3H_6}$ %
CrO/SiO_2	–	5:01	16.667	0.17	550	12.7	92.1	[37]
CrO/Al_2O_3	–	5:01	16.667	0.17	550	14	95.8	[37]
V_2O_3/Al_2O_3	–	2:05	70 cm^3/min		600	35	51	[126]
V_2O_3/SiO_2	–	2:05	70 cm^3/min		600	30	45	[126]
γ-Ga_2O_3	104	2.5:97.5	0.02	8	500	11.6	98.3	[133]
$Ga_8Al_2O_{15}$	119	2.5:97.5	0.02	8	500	22.5	98.2	[133]
$Ga_5Al_5O_{15}$	130	2.5:97.5	0.02	8	500	22.3	98	[133]
$Ga_2Al_8O_{15}$	147	2.5:97.5	0.02	8	500	21.9	97.2	[133]
Al_2O_3	173	2.5:97.5	0.02	8	500	0.6	84.2	[133]
Ga_2O_3/TiO_2	47	2.5:97.5	0.01	0.17	600	23	85	[56]
Ga_2O_3/Al_2O_3	102	2.5:97.5	0.01	0.17	600	33	92	[56]
Ga_2O_3/ZrO_2	19	2.5:97.5	0.01	0.17	600	39	74	[56]
Ga_2O_3/SiO_2	329	2.5:97.5	0.01	0.17	600	7.2	92	[56]
Ga_2O_3/MgO	35	2.5:97.5	0.01	0.17	600	5.3	34	[56]
$5In_2O_3/15Ga_2O_3/80Al_2O_3$	190	1:19	0.005	6	600	12.5	56.8	[136]
$10In_2O_3/10Ga_2O_3/80Al_2O_3$	174	1:19	0.0075	6	600	9	68.5	[136]
$15In_2O_3/5Ga_2O_3/80Al_2O_3$	160	1:19	0.01	6	600	7.5	49.5	[136]
$5In_2O_3/15Ga_2O_3/80Al_2O_3$	190	1:19	0.01	6	600	12.5	45	[136]
$10In_2O_3/10Ga_2O_3/80Al_2O_3$	174	1:19	0.01	6	600	12.5	35	[136]
$1Na_2O$-$20Cr_2O_3/Al_2O_3$	–	1:19	0.004	6	600	11.8	85	[136]
In-Al-40	94	2.5:97.5	0.02	12	600	12	80	[141]
In-Al-20	174	2.5:97.5	0.02	12	600	16	84	[141]
In-Al-10	195	2.5:97.5	0.02	12	600	14	86	[141]
$Mg_{0.15}V_2O_5.152.4H_2O/Al_2O_3$	–	2:05	70 cm^3/min		600	35	51	[126]
$Mg_{0.15}V_2O_5.152.4H_2O/SiO_2$	–	2:05	70 cm^3/min		600	25	45	[126]

(Inert in the feed composition represents Ar, He, or N_2, X = conversion, S = selectivity, and Y = yield).

will be enhanced by increasing the reaction temperature, therefore both temperature and pressure should be controlled to achieve high olefin yields.

It should be noted that process conditions are not limited to just temperature and pressure, other parameters such as feed composition, feed flow rate and reactor configuration are of equal importance. For example, micoporous membrane reactors coated with V-Mg-O and Ni nanoparticles have been shown to improve the propene yield at low C_3H_8/O_2 ratio under separate feeding configuration, in comparison to conventional fixed-bed reactors [144]. Moreover, the effect of CO_2 partial pressure on the conversion of propane is widely examined by various researchers. The general trend is that the increase in the partial pressure of CO_2 increases the conversion of propane and the formation of CO and H_2O, whereas reduces the formation of H_2 [26,51,56,58,145,146]. In ODPC reaction, about 50% of the H_2 formed is converted by the CO_2 [58]. Fig. 16 represents data reported for the effect of CO_2 partial pressure on the conversion of propane over Cr/MCM-41 catalysts prepared by direct hydrothermal method [36]. As can be seen, the rate of C_3H_6 and CO formation increased with

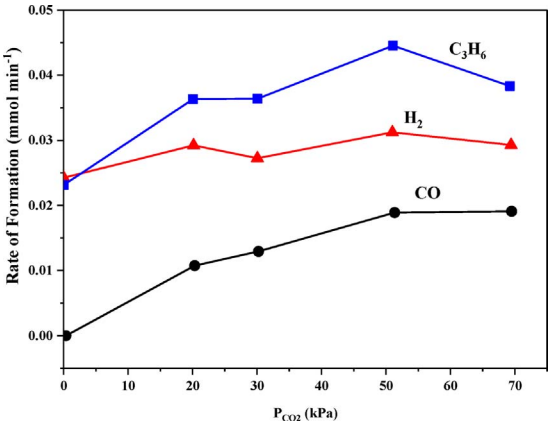

Fig. 16. CO_2 dehydrogenation of propane over Cr/MCM-41. Reaction conditions: catalyst weight = 400 mg; P (C_3H_8) = 12.2 kPa; P (CO_2) = 68.9 kPa; P (N_2) = 20.3 kPa; reaction temperature = 550 °C; F = 0.134 mol h^{-1} [36].

increasing the partial pressure of CO_2, while the rate of H_2 formation showed no significant change. The selectivity toward C_3H_6 was always around 95% and small amounts of C_2H_6, C_2H_4, and CH_4 were formed as well. This further confirms the essential role of CO_2 partial pressure in the propane dehydrogenation process.

The effect of CO_2 partial pressure on the activity of Cr/SiO_2 and Cr/Al_2O_3 was further investigated by Shishido et al. [36]. The activity of Cr/SiO_2 was enhanced with increasing the partial pressure of CO_2, while the activity of Cr/Al_2O_3 was remarkably reduced by adding a small amount of CO_2. Kinetic analyses suggested that CO_2 adsorbed on Al_2O_3 inhibites the adsorption of C_3H_8, thereby reducing the activity of Cr/Al_2O_3. Similar observation and explanation were offered by Michorczyk's group [37] for investigated Cr/SiO_2 and Cr/Al_2O_3 catalysts. More coke deposits were observed in the CO_2 environment than that in the N_2, highlighting that coke suppression was not the main role of CO_2. Nonetheless, CO formed from CO_2 during the dehydrogenation of C_3H_8 over Cr/SiO_2 and Cr/Al_2O_3. This could have resulted from the RWGS or reverse Boudouard reactions, but since more coke accompanied CO_2 addition, it may not be wrong to exclude the reverse Boudouard reactions in this case. The authors further investigated the possibility of optimizing CO and H_2 produced from ODPC reaction based on catalysis and thermodynamics analyses. A reaction mixture of propane at 14.5 kPa partial pressure and a varying amount of CO_2 with N_2 at flow rate of 30 cm^3 min^{-1} with varying reaction temperature were selected as the reaction conditions. Their results indicated that the equilibrium yield of propylene is much higher in the presence of CO_2 than in its absence, and similar yield as the commercialized dehydrogenation processes can be obtained at lower temperatures. Thermodynamic considerations pointed out that temperature has a much smaller effect on the equilibrium molar ratio of CO/H_2 compared to the initial feed composition of C_3H_8 and CO_2 with the higher ratio obtained at $CO_2/C_3H_8 > 1$. Over the investigated catalysts, propane conversion and propylene yield increased with increasing reaction temperature, while the selectivity to propylene dropped. Conversion was found to be significantly lower at temperatures below 823 K, whereas side reactions dominated above 873 K, leading to quick catalyst deactivation. The differences in results were accounted for by the interaction of CO_2 molecules with the catalysts.

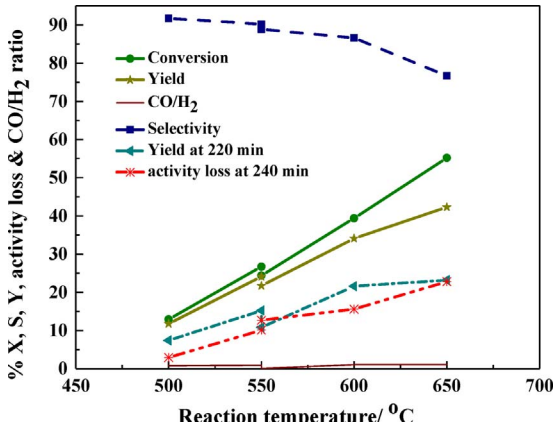

Fig. 17. Effect of temperature on catalytic performance of 0.04%Cr/SBA-1. Reaction conditions: molar ratio of CO_2:C_3H_8:He = 5:1:9; total flow rate = 30 $cm^3\ min^{-1}$; catalyst weight = 200 mg; reaction time = 10 min. Higher value at the step: with CO_2, lower value: without CO_2 [88].

The investigation of the influence of CO_2 partial pressure on the dehydrogenation reaction has suggested two roles of CO_2: a positive role of transforming H_2 into CO and H_2O through the RWGS reaction, and a negative role by blocking the dissociative adsorption of propane on the catalyst surface. The catalytic stability is also expected to improve by the addition of CO_2 to the feed gas due to the suppression of coke formation through the Bourdard reaction [86]. Aside from the transformation of H_2 and removal of coke, Ren et al. [86] reported that CO_2 promotes desorption of propylene. In another study [88], it was found that increase in molar ratio of CO_2/C_3H_8 results in the enhancement of the yield and selectivity to propylene and molar ratio of H_2/CO. The authors attributed this positive effect to direct oxidation of propane to propylene (Eq. (3)) in addition to the hydrogen consumption by the RWGS reaction (Eq. (2)), which shifts the propane dehydrogenation equilibrium. In effect, the use of CO_2 generates useful syngas whose amount can be controlled by regulating the feed gas composition.

Fig. 17 shows the performance of 0.04 wt% Cr/SBA-1 catalyst as a function of temperature in the presence of CO_2 [88]. Raising temperature from 550 to 650 °C increased the conversion of both propane and CO_2, and yield of propylene. However, the values decreased with time at each temperature. Except for activity loss, the rest of these parameters decreased when the catalyst was tested at 550 °C in the absence of CO_2 as indicated by the step in each line. The loss in activity with increase in temperature is attributed to coking (reversible deactivation) and loss of textural parameters (irreversible) of the Cr-catalyst. In addition, lattice oxygen consumption during ODPC reaction contributes to the deactivation of the catalyst. Coking often easily comes from propylene than propane, which could be the reason for the loss in selectivity [36].

Baek et al. [89] reported similar observations on temperature dependency of catalyst activity in ODPC reaction. The activity of catalysts increased with temperature, but selectivity dropped remarkably at 700 °C. Although higher temperature favors propylene formation, it also promotes catalyst sintering, agglomeration, and carbon deposition on active sites, thereby resulting in catalyst deactivation. High activity and acceptable selectivity were achieved at 600 °C, which was the most suitable reaction temperature for the reaction. The performance of dehydrogenation catalysts deteriorates with reaction time, so it is necessary to regenerate the catalysts frequently to retain sufficient activity. Therefore, optimum distribution and interaction of metal oxide particles with support as well as support with relatively large surface area and pore size are required to prevent sintering and aggregation after harsh hydrothermal conditions that the materials are exposed during regeneration process.

In summary, the effect of CO_2 partial pressure in promoting dehydrogenation of propane varies with catalyst type and nature of metal used. For easily oxidized metals such as Cr and V, CO_2 basically reoxidizes the reduced active species in the reaction process, whereas for metal species like Ga and In that are difficult to reduce even under oxidative conditions, the normal non-oxidative dehydrogenation occurs and CO_2 basically consumes the H_2 produced and hence induces positive equilibrium effect [35,36,62,64,83,129]. The role of CO_2 in ODP reaction including consumption of H_2, removal of coke, and desorption of propylene, has been consistent in the works published by many other researchers using different catalysts [35,36,84]. With respect to temperature, alkane dehydrogenation reactions are very complicated because they are thermodynamically limited at low temperatures and high pressures. At high temperatures where thermodynamics favor conversions, side reactions become dominant and selectivity to desired products decreases significantly. To enable an energy-efficient ODPC process with high efficiency, it is imperative to consider process conditions in addition to catalysts properties. In other words, a design platform should be established through which the design and creation of catalyst materials are informed by the process parameters and vise versa.

6. Summary and outlook

In this critical review, the current challenges and future opportunities of CO_2 utilization as a soft oxidant foe selective dehydrogenation of propane was presented and discussed. Oxidative dehydrogenation of light alkanes with CO_2 is a vibrant field that so far has not yielded commercially viable catalytic technology. Several types of catalysts (zeolites, zeolite-supported metal oxides, and mixed-metal oxides) have been extensively explored for ODPC reaction with some promising results that could bring the process one step closer to the commercialization. However, the role of CO_2 and the mechanism of the dehydrogenation reaction are not clearly documented over these heterogeneous catalysts and are much dependent on the nature of the catalyst and support material used. The coupling effect of dehydrogenation with the RWGS reaction has advanced the performance of some catalysts, while adversely affected the performance of others. Such opposing roles are not clearly explained in the reported literature. Catalyst deactivation by catalyst sintering and coke deposition represents additional challenges, as catalyst aggregation and coke deposition increase at higher reaction temperature and lower H_2 partial pressure, respectively. Redox catalyst deactivation is also caused by reduction of metal oxides, in which case CO_2 becomes a viable means of reactivating those catalysts. Other means include phase transformation of active phases to more stable ones and surface coverage by adsorbed hydrogen.

By reviewing the literature data, it appears that zeolite-supported metal oxide catalysts (bifunctional materials) will offer promising performance in the ODPC reaction through cooperative interaction between acid sites on zeolite and active metal centers which leads to improved stability and selectivity. Even though some work has been done on zeolite-supported reducible transition metals, more work is still needed to promote this cooperative interaction.

Despite significant progress within the past few years, the ODPC process still has a long way to go to become a commercially available technology. It appears that a bridge between catalyst chemists and engineers is crucial to fill the gap between characteristics of the catalysts and process performance. Future targets of research should focus on the advantageous properties of composite materials and breakthrough processes. Understanding the thermodynamics and kinetics of the ODPC reaction as well as RWGS pathways is necessary to enable the design of new catalysts with advanced catalytic properties. Progress is anticipated in the research areas of (i) bifunctional acid-base or acid-redox catalysis, and (ii) membrane reactors. Since the ODPC is an equilibrium-limited reaction, such thermodynamic constraint can be

partially alleviated by employing membrane reactors by which the catalyst is introduced to a membrane system with high thermal stability to remove molecules with smaller kinetic diameter from the reaction mixture and hence shifts the equilibrium for production of pure propylene. Currently, such systems have been comparatively less explored. Furthermore, a combination of *in-situ* characterization techniques and theoretical studies (*e.g.* DFT and kinetics energy) is necessary to identify and evaluate key reaction intermediates.

Acknowledgment

The authors acknowledge University of Missouri research board (UMRB) for financial support.

References

[1] J.J.H.B. Sattler, J. Ruiz-Martinez, E. Santillan-Jimenez, B.M. Weckhuysen, Chem. Rev. 114 (2014) 10613–10653.
[2] M.B. Ansari, S.-E. Park, Energy Environ. Sci. 5 (2012) 9419–9437.
[3] A.J.R. Castro, J.M. Soares, J.M. Filho, A.C. Oliveira, A. Campos, É.R.C. Milet, Fuel 108 (2013) 740–748.
[4] T. Badstube, H. Papp, P. Kustrowski, R. Dziembaj, Catal. Lett. 55 (2000) 169–172.
[5] M. Myint, B. Yan, J. Wan, J.G. Chen, J. Catal. 343 (2016) 168–177.
[6] E.V. Kondratenko, M. Cherian, M. Baerns, D. Su, R. Schlgl, X. Wang, I.E. Wachs, J. Catal. 234 (2005) 131–142.
[7] K. Nowińska, A. Wącław, A. Izbińska, Appl. Catal. A: Gen. 243 (2003) 225–236.
[8] S. Sugiyama, T. Osaka, Y. Hirata, K.-I. Sotowa, Appl. Catal. A: Gen. 312 (2006) 52–58.
[9] R. Bulánek, B. Wichterlová, K. Novoveská, V. Kreibich, Appl. Catal. A: Gen. 264 (2004) 13–22.
[10] F. Solymosi, P. Tolmacsov, K. Kedves, J. Catal. 216 (2003) 377–385.
[11] F. Solymosi, P. Tolmacsov, T.S. Zakar, J. Catal. 233 (2005) 51–59.
[12] Y. Ramesh, P. Thirumala Bai, B. Hari Babu, N. Lingaiah, K.S. Rama Rao, P.S.S. Prasad, Appl. Petrochem. Res. 4 (2014) 247–252.
[13] C. a Carrero, R. Schloegl, I.E. Wachs, R. Schomaecker, ACS Catal. 4 (2014) 3357–3380.
[14] M. Chen, J.-L. Wu, Y.-M. Liu, Y. Cao, L. Guo, H.-Y. He, K.-N. Fan, Appl. Catal. A: Gen. 407 (2011) 20–28.
[15] R. Grabowski, Catal. Rev. 48 (2006) 199–268.
[16] A.A. Rownaghi, D. Bhandari, S.K. Burgess, D.S. Mikkilineni, J. Appl. Polym. Sci. 134 (2017) 45418.
[17] A.A. Rownaghi, F. Rezaei, Y. Labreche, P.J. Brennan, J.R. Johnson, S. Li, W.J. Koros, ChemSusChem 8 (2015) 3439–3450.
[18] A.A. Rownaghi, A. Kant, X. Li, H. Thakkar, A. Hajari, Y. He, P.J. Brennan, H. Hosseini, W.J. Koros, F. Rezaei, ChemSusChem 9 (2016) 1166–1177.
[19] S.E. Kim, J. Urpelainen, Int. Environ. Agreem. Polit. Law Econ. 13 (2012) 411–423.
[20] D.-P. Häder, V.E. Villafañe, E.W. Helbling, Photochem. Photobiol. Sci. 13 (2014) 1370–1392.
[21] L.R. Boysen, V. Brovkin, V.K. Arora, P. Cadule, N. de Noblet-Ducoudré, E. Kato, J. Pongratz, V. Gayler, Earth Syst. Dyn. 5 (2014) 309–319.
[22] A. Al-Mamoori, A. Krishnamurthy, A.A. Rownaghi, F. Rezaei, Energy Technol. 5 (2017) 1–17.
[23] F. Rezaei, A.a. Rownaghi, S. Monjezi, R.P. Lively, C.W. Jones, Energy Fuels 29 (2015) 5467–5486.
[24] S. Kawi, Y. Kathiraser, Front. Energy Res. 3 (2015) 1–17.
[25] X. Du, B. Yao, S. Gonzalez-Cortes, V.L. Kuznetsov, H. AlMegren, T. Xiao, P.P. Edwards, Faraday Discuss. 183 (2015) 161–176.
[26] P. Michorczyk, P. Pietrzyk, J. Ogonowski, Microporous Mesoporous Mater. 161 (2012) 56–66.
[27] M.A. Botavina, Y.A. Agafonov, N.A. Gaidai, E. Groppo, V. Cortés Corberán, A.L. Lapidus, G. Martra, Catal. Sci. Technol. 6 (2016) 840–850.
[28] C. Yu, Q. Ge, H. Xu, W. Li, Catal. Lett. 112 (2006) 197–201.
[29] S. Vajda, M.J. Pellin, J.P. Greeley, C.L. Marshall, L.a. Curtiss, G.a. Ballentine, J.W. Elam, S. Catillon-Mucherie, P.C. Redfern, F. Mehmood, P. Zapol, Nat. Mater. 8 (2009) 213–216.
[30] O. Ovsitser, M. Cherian, A. Brückner, E.V. Kondratenko, J. Catal. 265 (2009) 8–18.
[31] K. Nakagawa, C. Kajita, K. Okumura, N. Ikenaga, M. Nishitani-Gamo, T. Ando, T. Kobayashi, T. Suzuki, J. Catal. 203 (2001) 87–93.
[32] P. Michorczyk, J. Ogonowski, Appl. Catal. A: Gen. 251 (2003) 425–433.
[33] R. Wu, P. Xie, Y. Cheng, Y. Yue, S. Gu, W. Yang, C. Miao, W. Hua, Z. Gao, Catal. Commun. 39 (2013) 20–23.
[34] N. Mimura, I. Takahara, M. Inaba, M. Okamoto, K. Murata, Catal. Commun. 3 (2002) 257–262.
[35] K. Nakagawa, C. Kajita, Y. Ide, M. Okamura, Catal. Lett. 64 (2000) 215–221.
[36] K. Takehira, Y. Ohishi, T. Shishido, T. Kawabata, K. Takaki, Q. Zhang, Y. Wang, J. Catal. 224 (2004) 404–416.
[37] P. Michorczyk, K. Ze, R. Niekurzak, J. Ogonowski, Pol. J. Chem. Technol. 14 (2012) 77–82.
[38] F. Cavani, N. Ballarini, A. Cericola, Catal. Today 127 (2007) 113–131.
[39] M.A. Botavina, G. Martra, Y.A. Agafonov, N.A. Gaidai, N.V. Nekrasov, D.V. Trushin, S. Coluccia, A.L. Lapidus, Appl. Catal. A: Gen. 347 (2008) 126–132.
[40] S. Wang, Z.H. Zhu, Energy Fuels 18 (2004) 1126–1139.
[41] X. Rozanska, R. Fortrie, J. Sauer, J. Am. Chem. Soc. 136 (2014) 7751–7761.
[42] S. Chakraborty, S.C. Nayak, G. Deo, Catal. Today 254 (2015) 62–71.
[43] B.V. Vora, Top. Catal. 55 (2012) 1297–1308.
[44] J.C. Bricker, Top. Catal. 55 (2012) 1309–1314.
[45] S. Albonetti, F. Cavani, F. Trifirò, Catal. Rev. 38 (1996) 413–438.
[46] O.V. Krylov, A.K. Mamedov, S.R. Mirzabekova, Ind. Eng. Chem. Prod. Res. Dev. 34 (1995) 474–482.
[47] F. Urlan, I.-C. Marcu, I. Sandulescu, Catal. Commun. 9 (2008) 2403–2406.
[48] H. Liu, Z. Zhang, H. Li, Q. Huang, J. Nat. Gas Chem. 20 (2011) 311–317.
[49] S.-W. Choi, W.-G. Kim, J.-S. So, J.S. Moore, Y. Liu, R.S. Dixit, J.G. Pendergast, C. Sievers, D.S. Sholl, S. Nair, C.W. Jones, J. Catal. 345 (2017) 113–123.
[50] B. Mo, N. Al, A. Siahvashi, D. Chester, A.A. Adesina, Ind. Eng. Chem. Res. 52 (2013) 4017–4026.
[51] M. Chen, J. Xu, Y.-M. Liu, Y. Cao, H.-Y. He, J.-H. Zhuang, Appl. Catal. A: Gen. 377 (2010) 35–41.
[52] F. Bustamante, R.M. Enick, A.V. Cugini, R.P. Killmeyer, B.H. Howard, K.S. Rothenberger, M.V. Ciocco, B.D. Morreale, S. Chattopadhyay, S. Shi, AIChE J. 50 (2004) 1028–1041.
[53] Z. Shen, J. Liu, H. Xu, Y. Yue, W. Hua, W. Shen, Appl. Catal. A: Gen. 356 (2009) 148–153.
[54] O.V. Krylov, A.K. Mamedo, S.R. Mirzabekova, Catal. Today 24 (1995) 371–375.
[55] S. Kawi, Y. Kathiraser, J. Ni, U. Oemar, Z. Li, E.T. Saw, ChemSusChem 8 (2015) 3556–3575.
[56] B. Xu, B. Zheng, W. Hua, Y. Yue, Z. Gao, J. Catal. 239 (2006) 470–477.
[57] J. Karuppiah, E.L. Reddy, M.S.P. Sudhakaran, S.B. Lee, Int. Conf. Renew. Energies Power Qual. (2016) 742–747.
[58] P. Michorczyk, P. Kuśtrowski, L. Chmielarz, J. Ogonowski, React. Kinet. Catal. Lett. 82 (2004) 121–130.
[59] C.W.R. Engelen, J.P. Wolthuizen, J.H.C. van Hooff, Appl. Catal. 19 (1985) 153–163.
[60] S. Zhang, Y. Zhou, Y. Zhang, L. Huang, Catal. Lett. 135 (2010) 76–82.
[61] S. Sahebdelfar, F.T. Zangeneh, Iran. J. Chem. Eng. 7 (2010) 51–57.
[62] Y. Sakurai, J. Catal. 209 (2002) 16–24.
[63] B. Xu, T. Li, B. Zheng, W. Hua, Y. Yue, Z. Gao, Catal. Lett. 119 (2007) 283–288.
[64] P. Michorczyk, P. Kuśtrowski, A. Kolak, M. Zimowska, Catal. Commun. 35 (2013) 95–100.
[65] H. Tsuneoka, K. Teramura, T. Shishido, T. Tanaka, J. Phys. Chem. C 114 (2010) 8892–8898.
[66] K. Pokrovski, K.T. Jung, A.T. Bell, Langmuir 17 (2001) 4297–4303.
[67] B. Bachiller-Baeza, I. Rodriguez-Ramos, A. Guerrero-Ruiz, Langmuir 14 (1998) 3556–3564.
[68] A.A. Rownaghi, F. Rezaei, J. Hedlund, Catal. Commun. 14 (2011) 37–41.
[69] A.A. Rownaghi, J. Hedlund, Ind. Eng. Chem. Res. 50 (2011) 11872–11878.
[70] A.A. Rownaghi, F. Rezaei, J. Hedlund, Microporous Mesoporous Mater. 151 (2012) 26–33.
[71] A.A. Rownaghi, F. Rezaei, J. Hedlund, Chem. Eng. J. 191 (2012) 528–533.
[72] A.A. Rownaghi, F. Rezaei, M. Stante, J. Hedlund, Appl. Catal. B: Environ. 119–120 (2012) 56–61.
[73] X. Li, A. Kant, Y. He, H.V. Thakkar, M.A. Atanga, F. Rezaei, D.K. Ludlow, A.A. Rownaghi, Catal. Today (2016) 1–16.
[74] Y. Li, Y. Huang, J. Guo, M. Zhang, D. Wang, F. Wei, Y. Wang, Catal. Today 233 (2014) 2–7.
[75] J.F. Haw, D.M. Marcus, Top. Catal. 34 (2005) 41–48.
[76] T. Armaroli, L.J. Simon, M. Digne, T. Montanari, M. Bevilacqua, V. Valtchev, J. Patarin, G. Busca, Appl. Catal. A: Gen. 306 (2006) 78–84.
[77] D. Uy, A.E. O'Neill, L. Xu, W.H. Weber, R.W. McCabe, Appl. Catal. B: Environ. 41 (2003) 269–278.
[78] H. Thakkar, A. Issa, A.A. Rownaghi, F. Rezaei, Chem. Eng. Technol. 40 (2017) 1–10.
[79] H. Thakkar, S. Eastman, A. Hajari, A.A. Rownaghi, J.C. Knox, F. Rezaei, ACS Appl. Mater. Interfaces 8 (2016) 27753–27761.
[80] H. Thakkar, S. Eastman, A. Al-Mamoori, A. Hajari, A.A. Rownaghi, F. Rezaei, ACS Appl. Mater. Interfaces 9 (2017) 7489–7498.
[81] P. Michorczyk, J. Ogonowski, P. Kuśtrowski, L. Chmielarz, Appl. Catal. A: Gen. 349 (2008) 62–69.
[82] L. Liu, H. Li, Y. Zhang, Catal. Commun. 8 (2007) 565–570.
[83] F. Zhang, R. Wu, Y. Yue, W. Yang, S. Gu, C. Miao, W. Hua, Z. Gao, Microporous Mesoporous Mater. 145 (2011) 194–199.
[84] Y. Ren, J. Wang, W. Hua, Y. Yue, Z. Gao, J. Ind. Eng. Chem. 18 (2012) 731–736.
[85] Q. Zhu, M. Takiguchi, T. Setoyama, T. Yokoi, J.N. Kondo, T. Tatsumi, Catal. Lett. 141 (2011) 670–677.
[86] Y. Ren, F. Zhang, W. Hua, Y. Yue, Z. Gao, Catal. Today 148 (2009) 316–322.
[87] H.J. Zhang, Z.G. Jia, S.F. Ji, Adv. Mater. Res. 287–290 (2011) 1671–1674.
[88] P. Michorczyk, J. Ogonowski, M. Niemczyk, Appl. Catal. A: Gen. 374 (2010) 142–149.
[89] J. Baek, H.J. Yun, D. Yun, Y. Choi, J. Yi, ACS Catal. 2 (2012) 1893–1903.
[90] L. Bai, Æ.Y. Zhou, Æ.Y. Zhang, Appl. Catal. (2009) 449–456.
[91] M. Tasbihi, F. Feyzi, M.A. Amlashi, A.Z. Abdullah, A.R. Mohamed, Fuel Process. Technol. 88 (2007) 883–889.
[92] Z. Nawaz, F. Wei, J. Ind. Eng. Chem. 16 (2010) 774–784.
[93] Y. Zhang, Y. Zhou, L. Huang, S. Zhou, X. Sheng, Q. Wang, C. Zhang, Chem. Eng. J. 270 (2015) 352–361.
[94] M. Razavian, S. Fatemi, Microporous Mesoporous Mater. 201 (2015) 176–189.
[95] Y. Zhang, Y. Zhou, Yian Li, Y. Wang, Y. Xu, P. Wu, Catal. Commun. 8 (2007)

1009–1016.
[96] Yiwei Zhang, Yuming Zhou, Kangzhen Yang, Yian Li, Yu Wang, Yi Xu, Peicheng Wu, Microporous Mesoporous Mater. 96 (2006) 245–254.
[97] Y. Zhang, Y. Zhou, M. Tang, X. Liu, Y. Duan, Chem. Eng. J. 181–182 (2012) 530–537.
[98] Y. Zhang, Y. Zhou, L. Huang, M. Xue, S. Zhang, Ind. Eng. Chem. Res. 50 (2011) 7896–7902.
[99] Z. Nawaz, X. Tang, Y. Chu, F. Wei, Chin. J. Catal. 31 (2010) 552–556.
[100] S.-J. Kim, Y. Liu, J.S. Moore, R.S. Dixit, J.G. Pendergast, D.S. Sholl, C.W. Jones, S. Nair, Chem. Mater. 28 (2016) 4397–4402.
[101] Y. Liu, J. Wang, G. Zhou, M. Xian, Y. Bi, K. Zhen, React. Kinet. Catal. Lett. 73 (2001) 199–208.
[102] A.A. Rownaghi, Y.H. Taufiq-yap, F. Rezaei, Ind. Eng. Chem. Res. 48 (2009) 7517–7528.
[103] K. Chen, A.T. Bell, E. Iglesia, J. Phys. Chem. B 104 (2000) 1292–1299.
[104] N.M. Schweitzer, B. Hu, U. Das, H. Kim, J. Greeley, L.a. Curtiss, P.C. Stair, J.T. Miller, A.S. Hock, ACS Catal. 4 (2014) 1091–1098.
[105] A.A. Rownaghi, Y.H. Taufiq-Yap, F. Rezaei, Chem. Eng. J. 165 (2010) 328–335.
[106] S. Tan, L.B. Gil, N. Subramanian, D.S. Sholl, S. Nair, C.W. Jones, J.S. Moore, Y. Liu, R.S. Dixit, J.G. Pendergast, Appl. Catal. A: Gen. 498 (2015) 167–175.
[107] W.-Z. Lang, C.-L. Hu, L.-F. Chu, Y.-J. Guo, RSC Adv. 4 (2014) 37107.
[108] S. Yang, E. Iglesia, A.T. Bell, J. Phys. Chem. B 109 (2005) 8987–9000.
[109] A.A. Rownaghi, Y.H. Taufiq-yap, Ind. Eng. Chem. Res. 49 (2010) 2135–2143.
[110] A.A. Rownaghi, Y.H. Taufiq-Yap, F. Rezaei, Catal. Lett. 130 (2009) 504–516.
[111] A.A. Rownaghi, Y.H. Taufiq-Yap, F. Rezaei, Chem. Eng. J. 155 (2009) 514–522.
[112] Y.A. Agafonov, N.A. Gaidai, A.L. Lapidus, Russ. Chem. Bull. 63 (2014) 381–388.
[113] Z. Zhai, X. Wang, R. Licht, A.T. Bell, J. Catal. 325 (2015) 87–100.
[114] A.A. Rownaghi, T.-Y.Y. Hin, T.W. Jiunn, Catal. Lett. 130 (2009) 593–603.
[115] Y.H. Taufiq-Yap, A.A. Rownaghi, M.Z. Hussein, R. Irmawati, Catal. Lett. 119 (2007) 64–71.
[116] C. Pak, A.T. Bell, T.D. Tilley, J. Catal. 206 (2002) 49–59.
[117] P. Michorczyk, J. Ogonowski, K. Zeńczak, J. Mol. Catal. A: Chem. 349 (2011) 1–12.
[118] J. a. Cecilia, C. García-Sancho, J.M. Mérida-Robles, J. Santamaría-González, R. Moreno-Tost, P. Maireles-Torres, Catal. Today 254 (2015) 43–52.
[119] K. Chen, A.T. Bell, E. Iglesia, J. Catal. 209 (2002) 35–42.
[120] G. Liu, Z.J. Zhao, T. Wu, L. Zeng, J. Gong, ACS Catal. 6 (2016) 5207–5214.
[121] A.H.S. Kootenaei, J. Towfighi, A. Khodadadi, Y. Mortazavi, Appl. Surf. Sci. 298 (2014) 26–35.
[122] J. Langanke, A. Wolf, J. Hofmann, K. Böhm, M.A. Subhani, T.E. Müller, W. Leitner, C. Gürtler, Green Chem. 16 (2014) 1865.
[123] Y.J. Du, Z.H. Li, K.N. Fan, J. Mol. Catal. A: Chem. 379 (2013) 122–138.
[124] Z. Zhao, C.-C. Chiu, J. Gong, Chem. Sci. 6 (2015) 4403–4425.
[125] F. Gilardoni, A.T. Bell, A. Chakraborty, P. Boulet, J. Phys. Chem. B 1225 (2000) 12250–12255.
[126] B.Y. Jibril, A.Y. Atta, K. Melghit, Z.M. El-Hadi, A.H. Al-Muhtaseb, Chem. Eng. J. 193–194 (2012) 391–395.
[127] M. Fattahi, F. Khorasheh, S. Sahebdelfar, F.T. Zangeneh, K. Ganji, M. Saeedizad, Sci. Iran. 18 (2011) 1377–1383.
[128] L. Guczi, Catal. Today 101 (2005) 53–64.
[129] L. Guczi, L. Bork, Fuel Energy Abstr. 40 (1999) 202.
[130] A.A. Lemonidou, M. Machli, Catal. Today 127 (2007) 132–138.
[131] R.Y. Saleh, I.E. Wachs, S.S. Chan, C.C. Chersich, J. Catal. 98 (1986) 102–114.
[132] D.A.H. Hanaor, C.C. Sorrell, J. Mater. Sci. 46 (2011) 855–874.
[133] M. Chen, J. Xu, F.Z. Su, Y.M. Liu, Y. Cao, H.Y. He, K.N. Fan, J. Catal. 256 (2008) 293–300.
[134] B. Zheng, W. Hua, Y. Yue, Z. Gao, J. Catal. 232 (2005) 143–151.
[135] Y. Cheng, H. Gong, C. Miao, W. Hua, Y. Yue, Z. Gao, Catal. Commun. 71 (2015) 42–45.
[136] S. Tan, S.-J. Kim, J.S. Moore, Y. Liu, R.S. Dixit, J.G. Pendergast, D.S. Sholl, S. Nair, C.W. Jones, ChemCatChem 8 (2016) 214–221.
[137] J.J.H.B. Sattler, I.D. Gonzalez-Jimenez, L. Luo, B. a Stears, A. Malek, D.G. Barton, B. a Kilos, M.P. Kaminsky, T.W.G.M. Verhoeven, E.J. Koers, M. Baldus, B.M. Weckhuysen, Angew. Chem. Int. Ed. Engl. (2014) 9251–9256.
[138] M. Chen, J. Xu, Y.L. Yong, H.H. Fan, J. Zhuang, Kang-nian, Catal. Lett. 124 (2008) 369–375.
[139] Y. Liu, Z.H. Li, J. Lu, K. Fan, J. Phys. Chem. C 112 (2008) 20382–20392.
[140] A.A. Gabrienko, S.S. Arzumanov, A.V. Toktarev, A.G. Stepanov, Chem. Phys. Lett. 496 (2010) 148–151.
[141] M. Chen, J. Xu, Y. Gao, H.-Y. He, K.-N. Fan, J.-H. Zhuang, J. Catal. 272 (2010) 101–108.
[142] J.A. Perdigon-Melon, A. Gervasini, A. Auroux, J. Catal. 234 (2005) 421–430.
[143] H. Li, Y. Yue, C. Miao, Z. Xie, W. Hua, Z. Gao, Catal. Commun. 8 (2007) 1317–1322.
[144] A. Pantazidis, J.A. Dalmon, C. Mirodatos, Catal. Today 25 (1995) 403–408.
[145] X. Shi, S. Ji, K. Wang, C. Li, Energy Fuels 22 (2008) 3631–3638.
[146] S. Kattel, W. Yu, X. Yang, B. Yan, Y. Huang, W. Wan, P. Liu, J.G. Chen, Angew. Chem. Int. Ed. Engl. 55 (2016) 1–7.